

$^{40}\text{Ar}/^{39}\text{Ar}$ and paleomagnetic constraints on the evolution of Volcán de Santa María, Guatemala

Rüdiger P. Escobar-Wolf^{1,†}, Jimmy F. Diehl^{1,§}, Brad S. Singer^{2,#}, and William I. Rose^{1,**}

¹Department of Geological and Mining Engineering and Sciences, Michigan Technological University, 1400 Townsend Drive, Houghton, Michigan 49931, USA

²Department of Geoscience, University of Wisconsin–Madison, 1215 West Dayton Street, Madison, Wisconsin 53706, USA

ABSTRACT

$^{40}\text{Ar}/^{39}\text{Ar}$ dating of 15 lava flows indicates that Volcán de Santa María grew episodically to 8 km³ in size at an average rate of 0.12 km³/ka between 103 and 35 ka. The composite cone grew in four phases, including two periods of intense activity at ca. 72 ka and ca. 35 ka, during which 1.5 km³ and 3 km³ of basaltic to andesitic magmas were erupted. There is no evidence of further volcanism after ca. 35 ka until the great dacitic eruption in 1902. The average eruptive rate is 0.16 km³/ka, if products of the 1902 eruption and subsequent Santiaguito dome are included. Whereas the Mono Lake excursion is not clearly recorded at Volcán de Santa María, as had been inferred from earlier studies, virtual geomagnetic poles (VGPs) of the 35 ka cone-forming lavas exhibit high-amplitude paleosecular variation that may correspond in time to the Mono Lake excursion. Two older packages of lava flows are each associated with a distinctive cluster of VGPs, which supports the $^{40}\text{Ar}/^{39}\text{Ar}$ age model and the conclusion that cone building was episodic. During the final 60% of cone growth, lavas evolved from basaltic to andesitic (51%–57% SiO₂) with time, but with a regression to slightly less evolved compositions during the onset of the final cone-building phase. Despite the relatively small volume of Santa María, cone-growth processes and geochemical evolution through time mirror observations at other currently active volcanoes along the Central American volcanic arc, and may prove useful as an analogy in assessing long-term hazards posed by other predominantly basaltic-andesitic composite volcanoes.

INTRODUCTION

The Santa María–Santiaguito volcanic complex near the western end of the Central American volcanic arc in the Guatemalan highlands (Fig. 1) includes the symmetrical composite cone of Volcán de Santa María and the east-west-elongated Santiaguito dome complex (Fig. 2). Santa María had been inactive with no historic eruptions recorded before 24 October 1902 when the second largest eruption of the twentieth century commenced from a vent on the southwest flank of the composite volcano, killing thousands of people and causing extensive damage to the Guatemalan economy

(Rose, 1972, 1987; Williams and Self, 1983; Sapper, 1904). In 1922 the Santiaguito volcanic complex began to grow inside the crater formed during the 1902 eruption and remains active, having erupted more than 1.2 km³ of dacitic magma (Harris et al., 2003; Durst, 2008).

The plinian phase of the 1902 eruption excavated a 0.5 km³ crater centered ~2.5 km southwest of the cone's 3772 masl summit (Fig. 2), exposing ~60% of the upper cone's volume (~5 km³) as a sequence of steeply dipping, interbedded lava flows and volcanoclastic layers (Fig. 3A). Analysis of hand specimens from 26 lava flows in this section by Rose et al. (1977) revealed a possible excursion of the geomagnetic

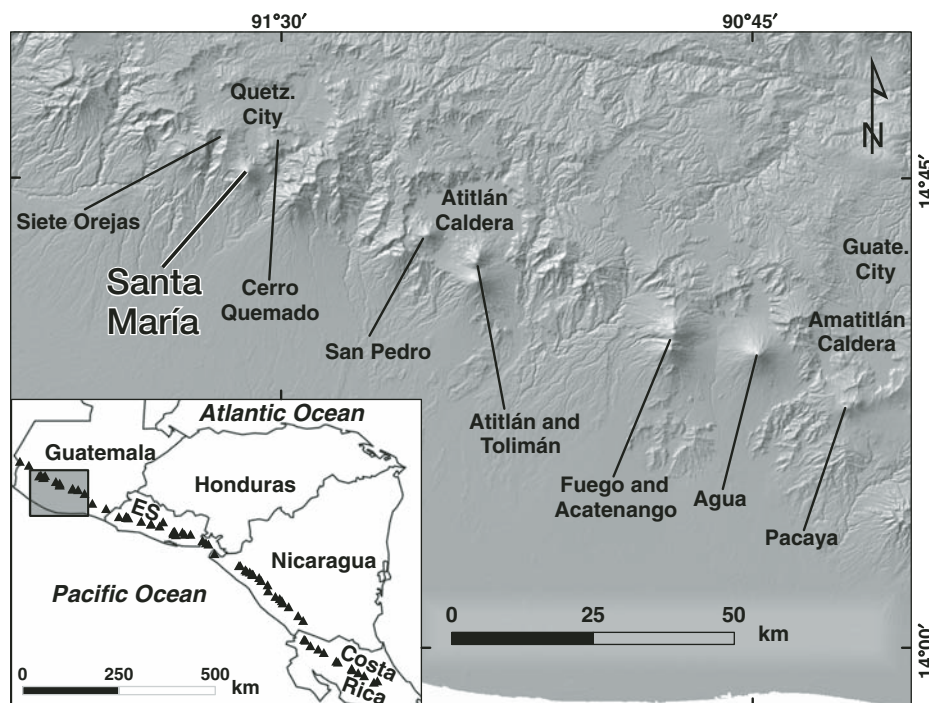


Figure 1. Location of the Santa María–Santiaguito volcanic complex within the northern part of the Central American volcanic arc (CAVA). Small triangles in the inset panel represent the 39 main volcanic centers (Carr et al., 2003). Abbreviations: ES—El Salvador; Quetz. City—Quetzaltenango City; Guate. City—Guatemala City.

[†]E-mail: rpescoba@mtu.edu

[§]E-mail: jdiehl@mtu.edu

[#]E-mail: bsinger@geology.wisc.edu

^{**}E-mail: raman@mtu.edu

Geology of Santa María volcano and surroundings

Qla Laharic and fluvial sediments from Santiaguigo and Santa María
Qal Alluvial deposits

Santiaguigo dome complex

SD Dacite lavas 1922–2007
c Caliente dome (active vent)
Im La Mitad dome
eb El Brujo dome
em El Monje dome

Cerro Quemado complex

Qll Llano del Pinal debris avalanche and blast deposit
Qcq Cerro Quemado dacite dome

Santa María composite volcano

Qsmf Flank lavas
 Basaltic-andesitic
Qsm Main cone 72–36 ka
 Basaltic-andesitic

Volcanoes older than Santa María

Qso Siete Orejas Volcano
Qwv Volcán del Valle
 Cinder cone
Qpa Pecul andesites
Qta Quaternary-Tertiary andesitic lava and breccia

Crater rim
 Major Fault Zone
 Road
 Sample locations (2005 and 2007)
 1902 crater wall (Fig. 3)
 Other sites
 Location of Conway et al. paleomagnetic section

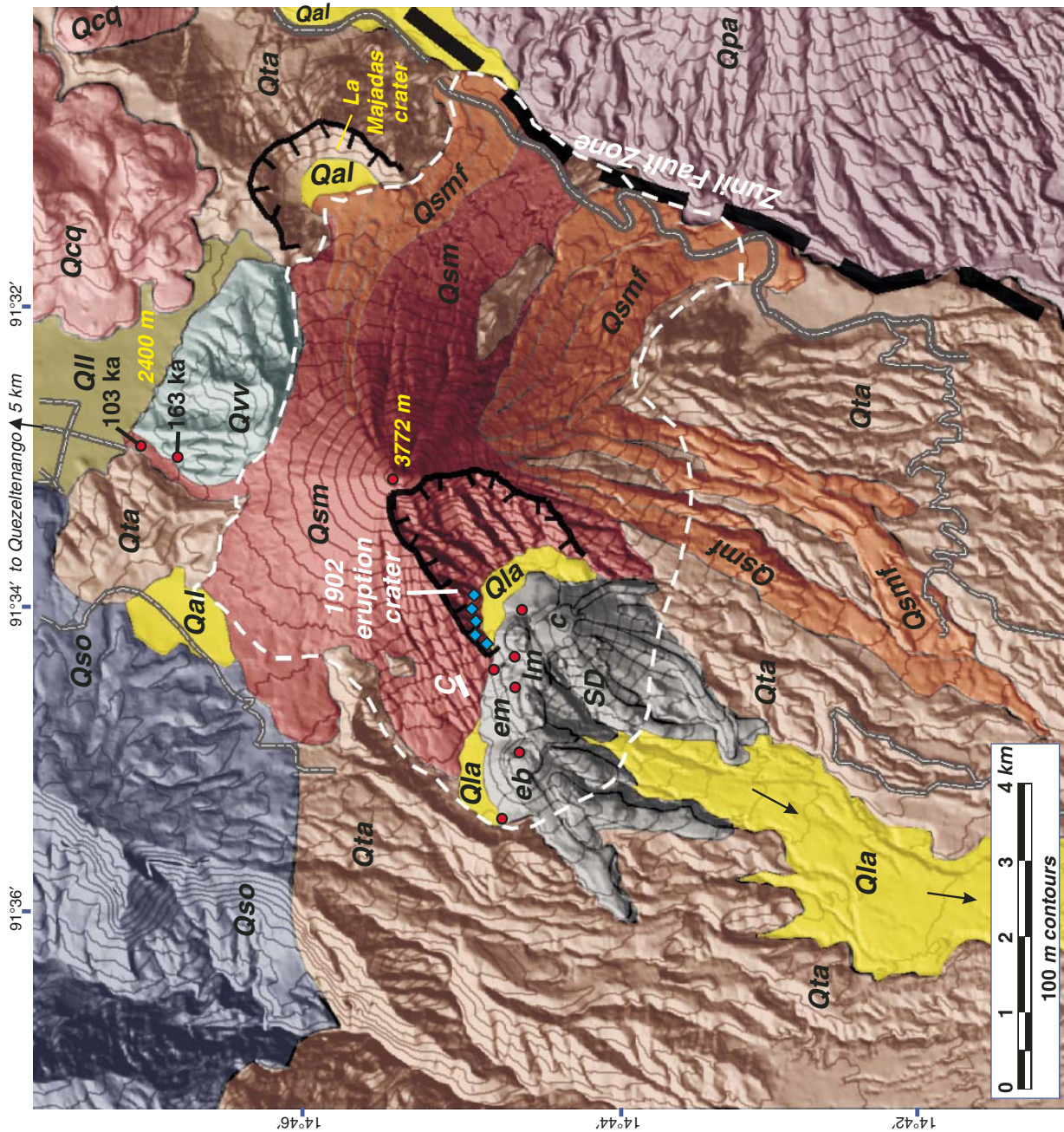


Figure 2. Geologic map of the Santa María-Santiaguigo volcanic complex. Geology modified from Rose (1987) and Conway et al. (1992) based on field observations in 2005, 2006, and 2007. The white dashed line shows the area of the cone that was considered for modeling the volume.

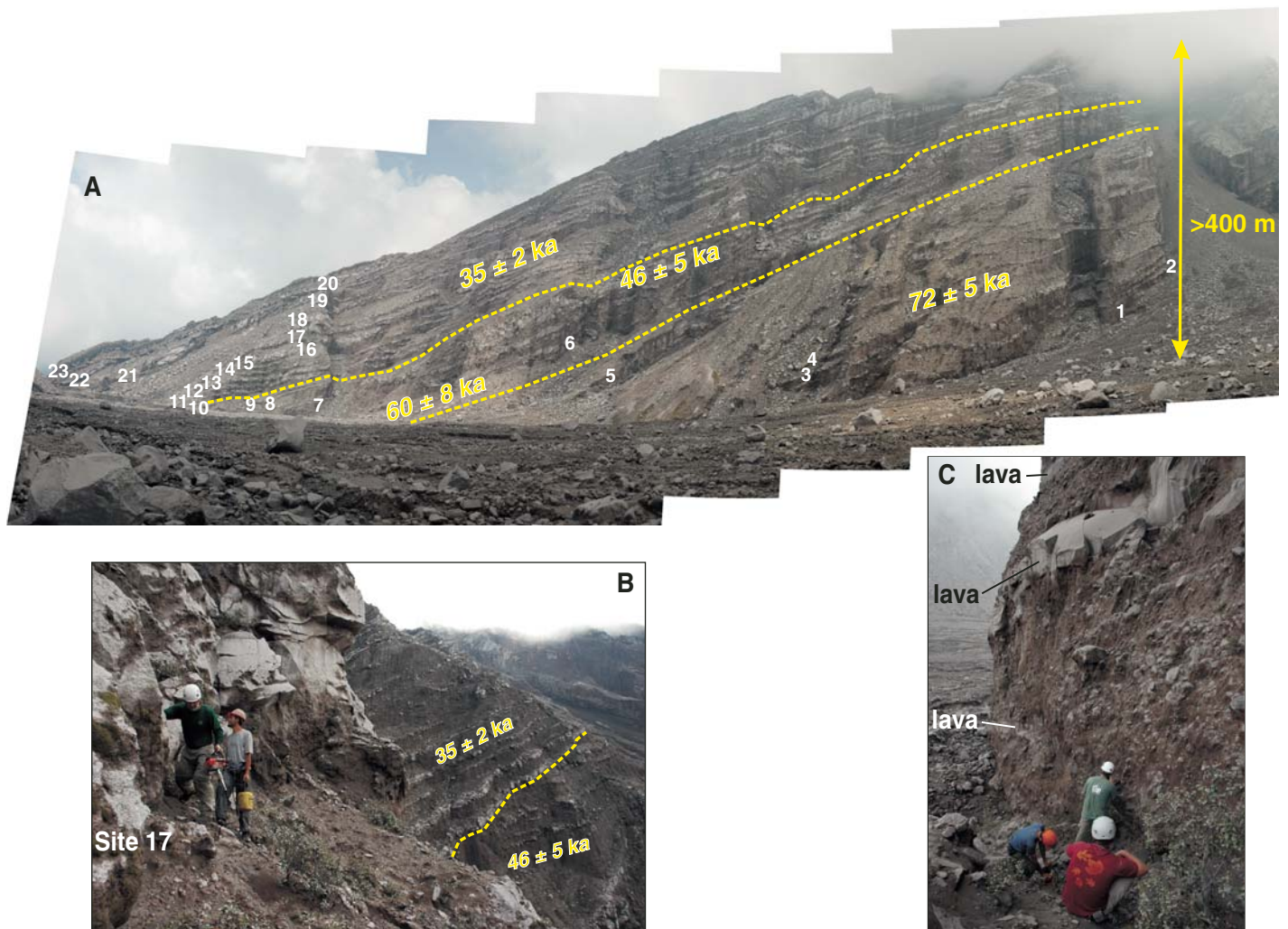


Figure 3. Stratigraphy of the Santa María cone. (A) Panoramic view, northwest wall of the 1902 Santa María eruption crater. Twenty-three paleomagnetic sample sites in lava flows are labeled (in white) from stratigraphically lowest to highest. The $^{40}\text{Ar}/^{39}\text{Ar}$ ages (in yellow) of 72 ± 5 , 60 ± 8 to 46 ± 5 , and 35 ± 2 ka determined for three packages of lava flows, separated by unconformities (dashed yellow lines) are shown with their uncertainties. The length along the base of the escarpment is 1 km. (B) View east along the escarpment from the position of site number 17 in panel A. The unconformity separating the middle and upper packages of lavas is along the dashed yellow line. (C) Alternating flows of lava and fragmental material at site number 2 in panel (A) above. The fragmental layers are mainly clast-supported and comprise a range of particle sizes from ash to 1-m-diameter blocks of mafic lava. Note also in panels (B) and (C) that the layers of fragmental material are typically much thicker, and two to three times more voluminous, than the relatively thin lava flows. Photographs by B.S. Singer, March 2005.

field and a trend of increasingly evolved lavas with stratigraphic position. Conway et al. (1994) correlated the apparent magnetic excursion with the Mono Lake excursion that had been ^{14}C dated at 28–25 ka (Liddicoat and Coe, 1979) and used this apparent geochronologic constraint to estimate eruptive rates.

The Mono Lake geomagnetic field excursion, originally discovered in sediments along Wilson Creek, near Mono Lake, California, USA (Denham and Cox, 1971; Liddicoat and Coe, 1979) has since been found in sedimentary records throughout the western United States (Liddicoat et al., 1982; Negrini et al., 1984; Lund et al., 1988; Levi and Karlin, 1989; Liddicoat,

1992, 1996; Rieck et al., 1992; Mankinen and Wentworth, 2004), Israel (Marco, 2002), India (Kotlia et al., 1997; Bhalla et al., 1998), and in sediments from the Atlantic and Arctic oceans and the Greenland Sea (Nowaczyk, 1997; Nowaczyk and Antonow, 1997; Nowaczyk and Knies, 2000; Laj et al., 2004; Channell, 2006). Correlation of the excursion with a local minimum in paleomagnetic intensity records from marine sediments, dated via comparison of oxygen isotopes to Greenland ice cores, allowed Laj et al. (2004) to determine an age of 34–35 ka for the Mono Lake excursion. Marine sediments at Ocean Drilling Program (ODP) site 919 reveal a clockwise and counterclockwise looping of

VGP paths that are astrochronologically dated at 40 and 33 ka, respectively, associated with the Laschamp and Mono Lake excursions (Channell, 2006). Moreover, Cassata et al. (2008) discovered that three excursional lava flows in the Auckland volcanic field, New Zealand, $^{40}\text{Ar}/^{39}\text{Ar}$ dated at 32 ± 2 ka, most probably record the Mono Lake excursion. Thus, despite recent challenges to the age and existence of the Mono Lake excursion (Kent et al., 2002; Zimmerman et al., 2006), this event has great potential as a global chronostratigraphic marker at 32–34 ka (Benson et al., 2003; Laj et al., 2004; Cassata et al., 2008).

The present study thus began with the aim to determine from oriented core samples collected

in situ and $^{40}\text{Ar}/^{39}\text{Ar}$ dating whether or not lava flows at Santa María record the Mono Lake excursion. A positive result could reveal with unusual detail the nature of this enigmatic feature of Earth's past magnetic field. We also kept in mind that studies of frontal arc volcanoes, which combine radioisotopic (K-Ar, $^{40}\text{Ar}/^{39}\text{Ar}$, and ^{14}C) dating with field mapping, stratigraphy, and volume estimates, emphasize the highly episodic nature of eruptions, complex compositional variability through time, and significant changes in eruption rates (Hildreth and Lanphere, 1994; Hildreth et al., 2003a, 2003b; Gamble et al., 2003; Singer et al., 1997, 2008; Frey et al., 2004; Bacon and Lanphere, 2006; Jicha and Singer, 2006; Hora et al., 2007). Access to exposures of lava flows and fragmental materials that comprise Santa María in the 1902 crater walls offers an opportunity unique in the Central American volcanic arc to quantify the long-term eruptive rate and magmatic evolution of a basaltic-andesitic composite cone typical of this arc.

We report new field observations, paleomagnetic directions, $^{40}\text{Ar}/^{39}\text{Ar}$ dating, and geochemical analyses of the lava flows exposed on the 1902 Santa María eruption crater walls, as well as ages for two flows on the main cone and one from an older, eroded, volcano, coupled with volume calculations. These data allow us to reconstruct the volcanic and magmatic history of Santa María, building upon previous efforts to understand hazards at this relatively simple but dangerous volcano.

GEOLOGY AND VOLCANOLOGY

Santa María–Santiaguito is one of 39 volcanic complexes that comprise the Central American volcanic arc, resulting from the subduction of the Cocos plate beneath the Caribbean plate (Carr et al., 2003) (Fig. 1). The volcanic complex is built upon 40- to 50-km-thick crust that may include Paleozoic basement rocks (Rose, 1987; Ligorría and Molina, 1997; Rebolgar et al., 1999; Carr et al., 2003). In Guatemala, basaltic to andesitic magmas have been erupted mainly from composite cones of the volcanic arc front, whereas dacitic to rhyolitic lavas and tuffs occur mainly in backarc calderas and dome complexes (Halsor and Rose, 1988). Several Quaternary to Holocene composite cones, domes, and calderas surround Santa María and have erupted subequal volumes of chemically bimodal mafic and silicic products (Rose et al., 1981; Rose, 1987). Volcanism at Santa María–Santiaguito is also bimodal, including roughly equal volumes of basaltic-andesitic ($\sim 8 \text{ km}^3$) and dacitic ($\sim 9 \text{ km}^3$) lava and tephra. The composite cone lavas (units *Qsm* and *Qsmf* in Fig. 2) are calc-alkalic, medium-K, and highly

sodic, and consist of two-pyroxene, olivine-bearing basalt to andesite. In stark contrast, the 1902 plinian eruption and subsequent extrusion of the Santiaguito dome complex (unit *SD* in Fig. 2) produced $\sim 9 \text{ km}^3$ of hornblende-dacite (Rose, 1987).

The 1902 crater exposures that are the main focus of this paper represent a remarkable, repetitive record of a typical “composite cone” (Davidson and De Silva, 2000). The crater sequence demonstrates an oscillatory pattern of massive basaltic-andesitic lava flows with fragmental layers (Fig. 3A). The overall quaquaversal dip is $\sim 33^\circ$. About two-thirds of the total thickness of the section is made of fragmental material and contains unsorted clasts ranging from fine ash all the way to boulders of lava (Figs. 3B and 3C). Many of the blocks have thermally fractured surfaces. Overall the material closely resembles “hot rockfalls” and block and ash-flow deposits. Although it is spectacularly better exposed at Santa María, the sequential oscillatory pattern exhibited is very similar to exposures on many other basaltic-andesitic composite cones, such as Fuego (Chesner and Rose, 1984), Atilán (Woodruff et al., 1979; Haapala et al., 2005), and Izalco (Carr and Pontier, 1981). We interpret these sequences as reflecting volcanic activity very similar to that shown by the currently active Fuego volcano, a composite cone almost the same height as Santa María and only 80 km to the SE (Martin and Rose, 1981; Fig. 1). Explosive eruptions of moderate size result in lava flows, often spatter fed, which flow from Fuego's central vent for variable distances, but break up into “hot rockfalls” and block and ash flows on the steep slopes. The variable eruption rates lead to flows of different lengths, and activity tends to be channeled for years to decades in sectors of the cone where cone growth produces oscillatory layers. These kinds of sequences are underreported and not well understood at composite volcanoes (Davidson and De Silva, 2000; Lyons et al., 2007), yet it seems likely that they are fundamental in the development of composite cones along the Central American volcanic arc and other arcs.

ANALYTICAL METHODS

Sampling

Twenty-three distinct lava flows exposed at sites on the walls of the 1902 eruption crater of Volcán de Santa María were sampled during field campaigns in 2005 and 2006. Guided by photographs taken by one of us (W.I.R.) in 1973, we attempted to sample the same lava flows as Rose et al. (1977), but aggradation of the crater floor due to mass wasting made it im-

possible to sample all of the previously exposed flows. At each site, four to seven one-inch-diameter cores up to three inches long were drilled for paleomagnetic analysis; an inadequate supply of water prevented more samples being drilled per site. Hand samples were collected for radioisotopic dating and geochemical analysis from the massive, unaltered interior of undisturbed lava flows. Drilled cores were oriented in situ using a magnetic compass, checked by sun compass readings. Relative stratigraphic positions were easily recognizable throughout the sequence (Fig. 3A). Site coordinates were obtained using a handheld global positioning system (GPS) device. Vertical distances between sites were measured using a 50-m tape normal to the dip of the lava flows. Although no major breaks in stratigraphy are evident in the crater walls, subtle unconformities observed during our fieldwork (Fig. 3B) most likely correspond with temporal gaps, suggesting that the lava flows may be grouped into three successive flow “packages” that include, successively, flows 1–5, 6–9, and 10–23 (Fig. 3A). $^{40}\text{Ar}/^{39}\text{Ar}$ geochronology discussed below further constrains time gaps between these packages.

In addition to the crater section of 23 flows, samples were collected in 2007 from Volcán del Valle (*Qvv*), a lava flow at 2660 masl at the base of the northern flank of the Santa María composite volcano (*Qsm*), and a lava from the summit of the composite cone at 3772 masl (*Qsm*; Fig. 2). The $^{40}\text{Ar}/^{39}\text{Ar}$ ages and compositions of these three lavas give a more complete perspective on the duration of eruptive activity than revealed from the crater section alone.

Paleomagnetic Work

Laboratory Procedures and Results

One-inch-long specimens were cut from the core samples drilled at each of the 23 lava flows in the 1902 crater section. The natural remnant magnetization (NRM) of each specimen was measured using a 2G Enterprises 760-R superconducting rock magnetometer equipped with an online alternating field (AF) demagnetization unit. Specimens were either subjected to AF (14–18 steps up to 140 mT) or thermal (5–13 heating steps up to 575 °C) demagnetization to isolate the characteristic direction of magnetization (ChRM) for each specimen. Secondary overprints were usually small or nonexistent and were easily removed in the first few steps of demagnetization, resulting in a linear decay of the magnetization vector to the origin on a vector endpoint diagram (Fig. 4). At several sites samples displayed great-circle paths with increasing levels of demagnetization. These samples came from sites located high on the

crater wall, suggesting their magnetization was partially reset by nearby lightning strikes. Characteristic direction of magnetization of all specimens was determined using principal component analysis (Kirschvink, 1980). Site-mean directions were calculated using either the statistical method of Fisher (1953) or the method of McFadden and McElhinny (1988) in

instances when the demagnetized data defined one or more remagnetization circles.

Alternating field and thermal demagnetization, as seen in Figure 4, of sister specimens from the same core isolate the same direction of magnetization. Maximum angular deviation (MAD) values using AF data are usually less than 1° , while MADs determined from thermal demagnetization are usually less than 3° . The difference in ChRMs determined by the two demagnetization techniques is always less than 10° and commonly less than 6° . At four sites where there were a sufficient number of two-specimen samples, the difference in the mean direction from thermal and AF demagnetized specimens is less than 5° . Therefore, we surmise that the ChRMs isolated using AF demagnetization represent a primary magnetization acquired during the initial cooling of these lava flows.

Site-mean directions, virtual geomagnetic poles, and associated statistical parameters calculated from the 23 lava flows are given in Table 1. Also listed in Table 1 are the data from Conway et al. (1994), obtained from sample sites in a short section ~1 km northwest of the crater wall section we sampled (Fig. 2). At some sites, a number of specimens were eliminated before calculating site-mean directions and VGPs. These specimens either had ChRMs that departed significantly (i.e., angular differences greater than 25°) from

the average of the specimens from that site or were from samples that were determined from the 2006 field season to have been drilled in rotated blocks; this resulted in the removal of four from a total of 122 samples in our data set.

The key results are that: (1) field directions are tightly clustered within each of the two lowermost lava packages; (2) these clusters differ from one another in mean direction; and (3) the stratigraphically highest lava package exhibits within the youngest half-dozen flows a large amplitude swing in direction (Figs. 5 and 6). These contrasts in magnetic field direction among the three lava packages most likely reflect secular variation, punctuated by temporal breaks, between the periods of eruptive activity that led to their emplacement (e.g., Hagstrum and Champion, 1995).

$^{40}\text{Ar}/^{39}\text{Ar}$ Dating

Analytical Procedures

Fifteen lava flows, including 12 of the 23 flows sampled for paleomagnetic study in Figure 3A, were $^{40}\text{Ar}/^{39}\text{Ar}$ -dated using furnace incremental-heating methods on groundmass separates at the Rare Gas Geochronology Laboratory at the University of Wisconsin–Madison. Sample preparation and analytical procedures are detailed in Singer et al. (2008). Three to four aliquots, 120–160 mg each, of groundmass from

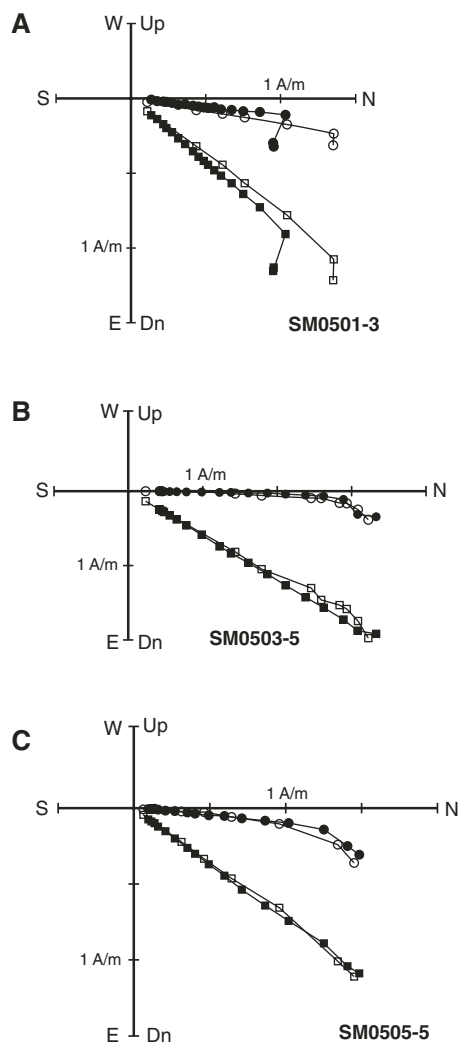


Figure 4. Vector endpoint diagrams of three Santa María lava specimens. Solid symbols correspond to alternating field (AF) demagnetization, and open symbols correspond to thermal demagnetization. Circles are projections onto the horizontal plane; squares are projections onto the N-S vertical plane. The demagnetization steps span from 0 to 575°C for the thermal demagnetization and from 0 to 140 mT for AF demagnetization for the samples shown. Both the AF and the thermal demagnetization yield virtually identical resultant directions, confirming the validity of the AF demagnetization approach.

TABLE 1. PALEOMAGNETIC DIRECTIONS

| Sample site | Inclination ($^\circ$) | Declination ($^\circ$) | N* | α_{95}^\dagger ($^\circ$) | κ^\ddagger | VGP | | Age (ka) |
|------------------|--------------------------|--------------------------|----|------------------------------------|-------------------|-------------------------------|--------------------------------|-----------------|
| | | | | | | Latitude ($^\circ\text{N}$) | Longitude ($^\circ\text{W}$) | |
| SM0501 | 34.5 | 8.0 | 6 | 6.2 | 154 | 81.28 | 327.98 | 75.0 ± 11.0 |
| SM0502 | 32.6 | 2.7 | 7 | 6.5 | 88 | 86.06 | 309.54 | 70.5 ± 7.3 |
| SM0503 | 29.8 | 2.6 | 6 | 3.7 | 334 | 87.22 | 331.23 | |
| SM0504 | 26.7 | 1.5 | 6 | 3.8 | 312 | 88.46 | 22.50 | 75.0 ± 13.0 |
| SM0505 | 39.9 | 359.0 | 5 | 3.0 | 491 | 82.39 | 268.4 | 71.3 ± 9.2 |
| SM0506 | -1.8 | 16.5 | 6 | 3.5 | 302 | 68.16 | 42.67 | 60.2 ± 8.1 |
| SM0507 | 8.6 | 17.0 | 6 | 4.8 | 199 | 70.25 | 28.67 | 53.9 ± 6.8 |
| SM0508 | 1.9 | 17.8 | 7 | 4.1 | 218 | 67.63 | 34.93 | |
| SM0509 | 4.2 | 11.1 | 5 | 5.4 | 200 | 73.27 | 46.54 | 46.0 ± 5.0 |
| SM0510 | 0.7 | 16.3 | 5 | 6.9 | 122 | 68.40 | 38.79 | |
| SM0511 | -2.6 | 16.7 | 5 | 1.6 | 2642 | 66.99 | 41.28 | |
| SM0512 | -2.5 | 17.8 | 5 | 3.4 | 508 | 66.19 | 39.15 | |
| SM0513 | 1.7 | 13.3 | 5 | 7.3 | 111 | 70.89 | 43.80 | 37.8 ± 4.9 |
| SM0514 | -8.3 | 23.1 | 3 | 2.8 | 1981 | 60.33 | 36.27 | |
| SM0515 | -12.0 | 18.4 | 5 | 3.9 | 380 | 62.35 | 45.98 | 35.4 ± 5.6 |
| SM0516 | -7.1 | 15.3 | 5 | 4.6 | 275 | 66.25 | 47.68 | |
| SM0517 | -9.4 | 9.0 | 6 | 3.1 | 468 | 68.54 | 63.09 | |
| SM0518 | 57.8 | 8.5 | 5 | 2.1 | 1358 | 65.18 | 284.43 | |
| SM0520 | 33.3 | 20.6 | 4 | 8.4 | 221 | 69.96 | 345.74 | 33.1 ± 3.7 |
| SM0521 | 23.4 | 17.7 | 5 | 4.2 | 389 | 72.61 | 4.67 | |
| SM0522 | 35.5 | 16.8 | 6 | 3.8 | 412 | 73.19 | 339.11 | 36.5 ± 4.6 |
| SM0523 | 28.1 | 17.9 | 5 | 9.6 | 84 | 72.70 | 355.44 | 36.8 ± 4.4 |
| SM1 [†] | 60.9 | 11.8 | 6 | 5.9 | 147 | 60.96 | 286.70 | |
| SM2 [†] | 60.9 | 20.6 | 6 | 4.2 | 289 | 57.51 | 297.59 | |
| SM3 [†] | 60.2 | 15.7 | 7 | 4.4 | 194 | 60.31 | 292.73 | |
| SM4 [†] | 57.4 | 8.9 | 5 | 4.9 | 240 | 65.43 | 285.48 | |
| SM5 [†] | 58.0 | 6.6 | 5 | 3.0 | 820 | 65.38 | 280.87 | |
| SM6 [†] | 28.7 | 13.8 | 5 | 3.4 | 781 | 76.66 | 354.23 | |
| SM7 [†] | 35.7 | 14.1 | 7 | 3.0 | 419 | 75.64 | 336.00 | |
| SM8 [†] | 6.1 | 344.0 | 7 | 3.4 | 314 | 70.37 | 143.43 | |

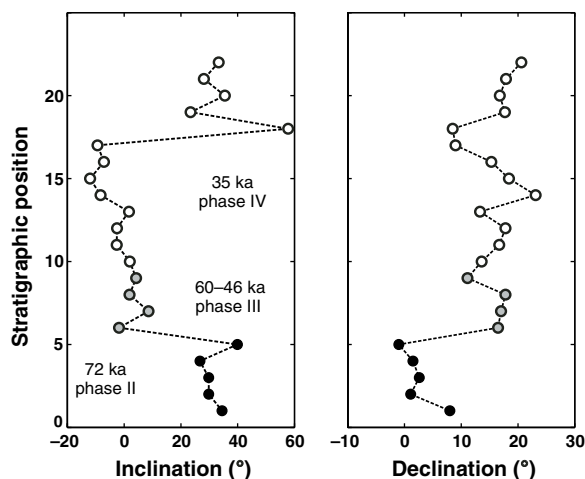
Note: *N is the number of specimens analyzed for each site (lava flow); VGP—virtual geomagnetic poles.

[†] α_{95} is the 95% confidence interval (angular) around the mean value.

[‡] κ is the Fisher (1953) precision parameter.

^{††}Data taken from Conway et al. (1994).

Figure 5. Paleomagnetic inclination and declination versus stratigraphic position for the 23 lava flow sites in the 1902 crater wall (Fig. 3A). See text for source of ages of the three lava packages, denoted by different symbols that define cone-building phases II, III, and IV.



each sample were degassed in 10–15 increments (620–1250 °C). Ages are calculated mainly relative to 1.194 Ma Alder Creek sanidine or, in four experiments, the 28.34 Ma Taylor Creek sanidine; these standards are closely intercalibrated with one another (Renne et al., 1998). During four analytical sessions that spanned more than one year, instrumental mass discrimination was measured using an air pipette every two to three days and varied between 1.0025 and 1.0076 per atomic mass unit. Furnace blanks were measured between samples at 200 °C increments covering the range of temperature used to degas the samples and interpolated to match temperatures at which samples were measured. Blanks were at least an order of magnitude smaller than sample signals, thus they contribute little to overall age uncertainties that are reported at the $\pm 2\sigma$ level of analytical precision.

A total of 48 incremental-heating experiments was done on the 15 lavas with two to four replicate plateau and isochron ages determined from subsamples of each lava flow (Fig. 7). Isochron regressions indicate an atmospheric trapped component in all but one sample (Table 2), but the spread in $^{40}\text{Ar}/^{39}\text{Ar}$ ratios along the isochrons is very limited. These factors lead us to take the inverse-variance weighted mean plateau ages to give the best estimate for time since eruption for 14 of the lava flows. Sample SM-07-08 from Volcán del Valle yields a mean $^{40}\text{Ar}/^{36}\text{Ar}$ value of 298.0 ± 2.1 that is slightly higher than atmosphere, thus for this sample we adopt the mean isochron age from the two experiments (Table 2).

Results

The ages range from 163.0 ± 49.0 to 33.1 ± 3.7 ka with the two oldest being the 163 ka lava from the deeply eroded Volcán del Valle and a 103 ka lava from near the base of the northern flank of the Santa María cone (Fig. 2). If the lava

dated at 103 ka is correctly attributed to the Santa María composite volcano, then contrary to Conway et al. (1994), the inception of cone-building predates the eruption of the ca. 84 ka Los Chocoyos tuff from the Atitlán caldera (Fig. 1) by nearly 20 ka. No deposits of Los Chocoyos ash are found on the flanks of the Santa María cone, nor does it clearly underlie any part of it that we have observed, making an independent test of the 103 ka age determination a challenge. Ages of samples from the upper part of the Santa María cone, including those from the 1902 crater section and the summit, are consistent with stratigraphic superposition, given the analytical uncertainties (Table 2). These latter ages fall into three groups that coincide with the unconformities and lava packages noted earlier. The oldest group comprises four age determinations between 75.0 ± 13.0 and 70.5 ± 7.3 ka; given that these ages are indistinguishable from one another, and they record a common paleomagnetic direction, the time span recorded is probably no longer than our best analytical uncertainty. Thus, we take the weighted mean age of these four lavas, 72 ± 5 ka, to estimate the time elapsed since eruption of this package that includes flow units 1–5 (Fig. 3A). The next highest package of four lava flows (sites 6–9) and intercalated fragmental material is characterized by a wider range of ages; from oldest to youngest these are 60.2 ± 8.1 , 53.9 ± 6.8 , and 46.0 ± 5.0 ka (Table 2; Fig. 3A). This middle package is overlain unconformably by a sequence of more than a dozen lava flows (sites 10–23) and fragmental materials that dip $\sim 33^\circ$ westward away from, but include, the summit lava flows. Six ages, including five from the crater section plus the lone summit lava sample, range from 38.0 ± 12.0 to 33.1 ± 3.7 ka and are indistinguishable from one another. As for the oldest lava package, we take the weighted mean age and uncertainty of these closely grouped

ages, 35 ± 2 ka, to give the best estimate of time elapsed since the latest preserved pulse of composite cone growth occurred.

To summarize, based in part on clustering of $^{40}\text{Ar}/^{39}\text{Ar}$ ages within lava packages, we can subdivide growth of the Santa María composite cone into four phases. Phase I began as the cone grew upon deeply eroded, ca. 163 ka remnants of Volcán del Valle at ca. 103 ka. Phase II occurred at 72 ± 5 . Phase III lavas and fragmental materials were deposited unconformably on the phase II products between ~ 60 and 46 ka. Phase IV, the final period of cone building, took place 35 ± 2 ka, as a voluminous sequence of lava flows and fragmental material was deposited unconformably over the phase III materials (Fig. 3A). The $^{40}\text{Ar}/^{39}\text{Ar}$ age determinations are consistent not only with stratigraphic observations but also paleomagnetic and geochemical findings outlined below.

Major and Trace Element Geochemistry

The cone-building basaltic to andesitic lavas are porphyritic and commonly contain $>35\%$ phenocrysts of plagioclase, augite, orthopyroxene, olivine, and titanomagnetite in a mainly holocrystalline matrix of the same phases plus minor glass (Rose et al., 1977; Rose, 1987). Whole-rock samples from the 23 flows in the crater section (SM-05-prefix), plus nine flows from Conway et al. (1994), were analyzed for major and trace elements by X-ray fluorescence (XRF) and inductively coupled plasma-mass spectrometry (ICP-MS) at Michigan State University following procedures in Vogel et al. (2006). Samples SM-07-01, -07, and -08, from the summit of Santa María, its northern flank, and Volcán del Valle (Fig. 2), were analyzed by XRF and ICP-MS for major and trace elements at the Open University using procedures in Rogers et al. (2006).

The lava compositions (GSA Data Repository Table DR1¹) range from basalt (50.7% SiO_2) to andesite (56.7% SiO_2), are generally consistent with earlier analyses by Rose et al. (1977) and Rose (1987), and exhibit in Harker-type variation diagrams a relatively coherent trend toward more evolved compositions over time (Fig. 8). In detail, the 103 ka phase I lava contains 53.7% SiO_2 , 4.8% MgO , 1.2% K_2O , 130 ppm Zr, and 23 ppm Rb, whereas younger ca. 72 ka lavas of phase II in the crater section are much lower in SiO_2 and contain on average 5.7% MgO , 0.7%

¹GSA Data Repository item 2010018, Major and trace element analyses of whole-rock lava samples from Volcán de Santa María, is available at <http://www.geosociety.org/pubs/ft2010.htm> or by request to editing@geosociety.org.

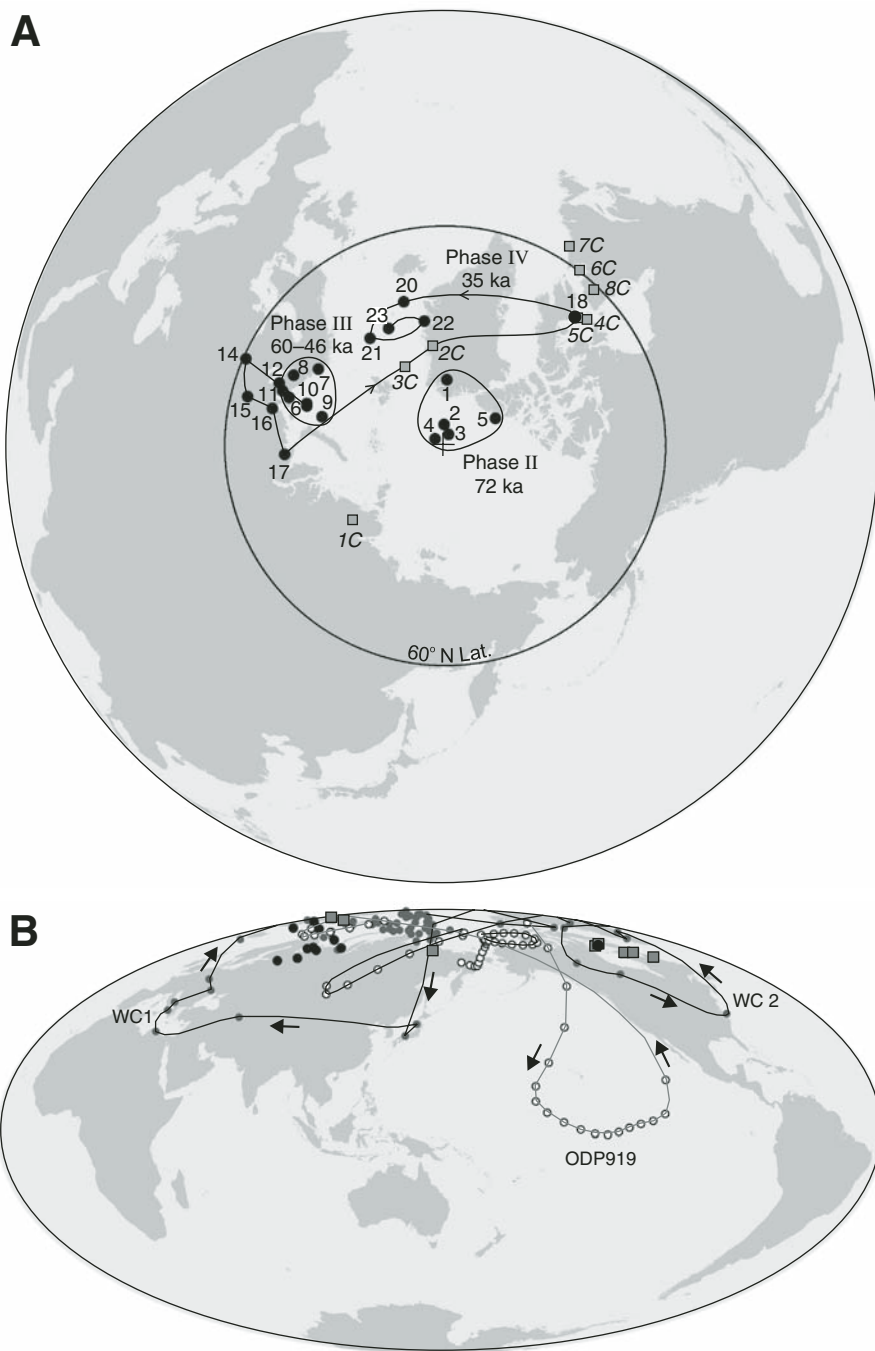


Figure 6. Virtual geomagnetic pole (VGP) positions corresponding to paleomagnetic directions. (A) Northern Hemisphere orthographic polar projection. Solid numbered circles show VGPs of lavas from the 1902 crater sequence (Fig. 3; Table 1). Gray squares labeled 1–8C are VGPs from data of Conway et al. (1994). The VGPs fall into three groups corresponding to the indicated phases of cone building. Note that the VGPs from Conway et al. (1994) are strikingly similar to those from the younger part of the phase IV lava package. (B) Hammer-Aitoff world projection of VGPs. Black circles and gray squares are from Santa María phase IV lavas dated at 35 ± 2 ka, and the gray squares show the Conway et al. (1994) data. Successive clockwise (WC1) and counterclockwise (WC2) loops are data from Liddicoat and Coe (1979) from the Wilson Creek Formation, Mono Lake, California. Also shown in open circles is the counterclockwise looping VGP path recovered from marine sediments deposited between ~ 36 and 30 ka at Ocean Drilling Program (ODP) site 919, North Atlantic Ocean (data from Channell, 2006).

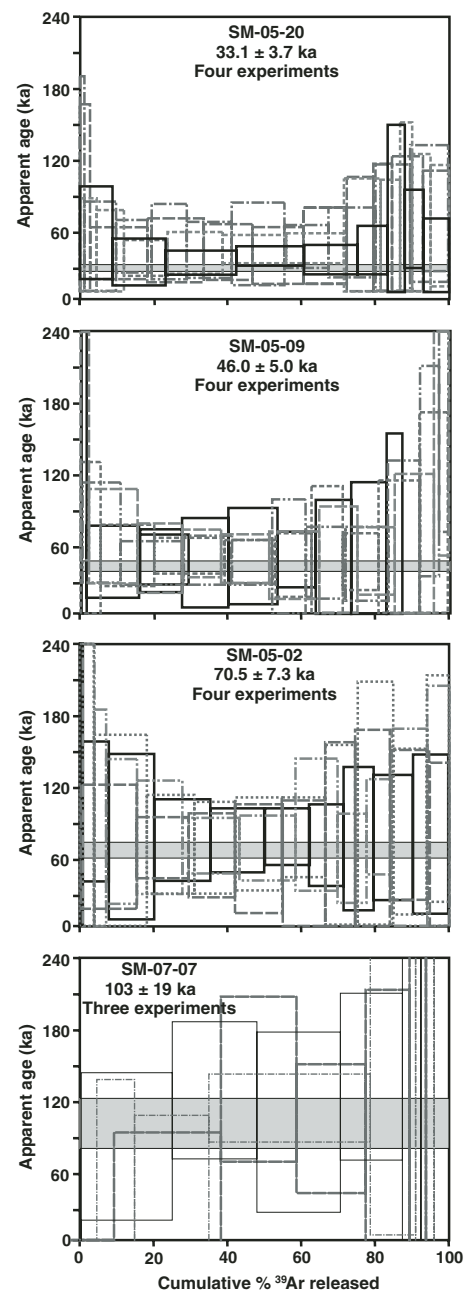


Figure 7. Age spectrum diagrams from four representative Santa María samples. Although results for individual gas steps are relatively imprecise, the weighted mean of the plateau ages in the multiple experiments done on each sample yields precise ages with 2σ analytical uncertainties indicated by the horizontal gray bands. The number of experiments corresponds to the number of replicate incremental-heating degassing and measurement experiments, done on individual aliquots of groundmass separates, from the same sample.

TABLE 2. SUMMARY OF 48 ⁴⁰Ar/³⁹Ar INCREMENTAL-HEATING EXPERIMENTS ON GROUNDMASS FROM 15 LAVA FLOWS

| Sample number Experiment | GPS coordinates (WGS 84 datum) | | Elevation (masl) | Weight (mg) | K/Ca total | Total fusion | | Age spectrum | | Isochron analysis | | |
|-----------------------------|--------------------------------|------------------------------|---------------------|----------------|---------------|----------------------------|----------|--------------|------|--|-----------------|-------------|
| | Latitude (deg min.ddd N) | Longitude (deg min.ddd W) | | | | Age ±2σ (ka) | MSWD | N | MSWD | ⁴⁰ Ar/ ³⁹ Ar ±2σ | Age ±2σ (ka) | |
| <u>SM-07-01</u> | 14 45.435 | 91 33.110 | 3770 | 129 | 0.1 | 201.5 ± 44.5 | 700–1075 | 85.3 | 0.19 | 6 of 9 | 296 ± 2.4 | 32.8 ± 61.4 |
| UW64F102 | | | | 161 | 0.14 | 119.6 ± 29.2 | 950–1150 | 52.2 | 0.23 | 3 of 8 | 296 ± 2.5 | 24.1 ± 60.9 |
| UW66A1 | | | | 155 | 0.14 | 98.4 ± 26.0 | 850–1150 | 58.9 | 0.51 | 5 of 8 | 297 ± 3.3 | 23.3 ± 29.9 |
| UW66A2 | | | | | | Weighted mean plateau age: | | | | 14 of 26 | | |
| <u>SM-05-20</u> | 14 44.912 | 91 34.170 | 2403 | 122 | 0.26 | 34.4 ± 12.9 | 721–1250 | 88.6 | 0.04 | 8 of 10 | 295.7 ± 3.7 | 30.6 ± 17.6 |
| UW55C2B | | | | 122 | 0.24 | 40.7 ± 12.7 | 718–1250 | 76.7 | 0.05 | 6 of 10 | 295.6 ± 10.0 | 35.3 ± 36.5 |
| UW55C1B | | | | 128 | 0.26 | 39.9 ± 10.2 | 650–1200 | 82.4 | 0.2 | 7 of 12 | 294.6 ± 5.7 | 39.1 ± 19.7 |
| UW55C1T | | | | 123 | 0.26 | 36.5 ± 8.6 | 680–1200 | 74.2 | 0.33 | 5 of 10 | 296.5 ± 6.8 | 28.2 ± 20.8 |
| UW55C2T | | | | | | Weighted mean plateau age: | | | | 26 of 42 | | |
| <u>SM-05-23</u> | 14 44.818 | 91 34.243 | 2294 | 120 | 0.24 | 43.9 ± 12.2 | 755–1265 | 81.3 | 0.12 | 7 of 10 | 296.7 ± 4.3 | 28.9 ± 15.5 |
| UW55C5B | | | | 122 | 0.24 | 54.8 ± 14.6 | 771–1300 | 80 | 0.01 | 7 of 11 | 296.2 ± 13.0 | 40.7 ± 40.5 |
| UW55C6T | | | | 121 | 0.24 | 39.6 ± 9.8 | 670–1230 | 92.1 | 0.04 | 8 of 11 | 295.9 ± 4.3 | 37.0 ± 15.4 |
| UW55C5T | | | | | | Weighted mean plateau age: | | | | 22 of 32 | | |
| <u>SM-05-22</u> | 14 44.834 | 91 34.222 | 2299 | 121 | 0.25 | 44.5 ± 10.4 | 763–1230 | 90.6 | 0.04 | 8 of 10 | 296.1 ± 4.0 | 35.1 ± 17.4 |
| UW55C3B | | | | 121 | 0.25 | 35.9 ± 13.0 | 778–1230 | 96.1 | 0.04 | 9 of 10 | 295.3 ± 2.2 | 36.0 ± 14.9 |
| UW55C4T | | | | 120 | 0.24 | 37.0 ± 10.8 | 670–1230 | 99.6 | 0.07 | 10 of 11 | 295.8 ± 1.8 | 34.2 ± 11.8 |
| UW55C3T | | | | | | Weighted mean plateau age: | | | | 27 of 31 | | |
| <u>SM-05-15</u> | 14 44.872 | 91 34.165 | 2351 | 122 | 0.23 | 48.1 ± 12.8 | 768–1250 | 86.8 | 0.09 | 7 of 10 | 295.9 ± 4.4 | 35.7 ± 23.9 |
| UW55B6B | | | | 121 | 0.21 | 46.3 ± 12.8 | 768–825 | 85.4 | 0.04 | 7 of 10 | 295.5 ± 5.1 | 32.3 ± 28.1 |
| UW55B5B | | | | 120 | 0.21 | 38.8 ± 12.9 | 650–1310 | 92.1 | 0.03 | 8 of 12 | 295.8 ± 2.9 | 34.6 ± 20.3 |
| UW55B5T | | | | | | Weighted mean plateau age: | | | | 22 of 32 | | |
| <u>SM-05-13</u> | 14 44.853 | 91 34.157 | 2330 | 127 | 0.22 | 42.1 ± 13.0 | 742–1210 | 91.6 | 0.08 | 8 of 10 | 296.4 ± 6.4 | 36.7 ± 25.9 |
| UW55B3B | | | | 126 | 0.21 | 43.0 ± 12.6 | 766–1220 | 91 | 0.14 | 8 of 11 | 295.5 ± 5.7 | 38.7 ± 20.5 |
| UW55B4T | | | | 122 | 0.22 | 42.1 ± 10.2 | 650–1220 | 97.1 | 0.12 | 10 of 12 | 295.7 ± 3.4 | 35.9 ± 14.9 |
| UW55B3T | | | | | | Weighted mean plateau age: | | | | 26 of 33 | | |
| <u>SM-05-09</u> | 14 44.837 | 91 34.118 | 2313 | 124 | 0.27 | 56.3 ± 13.6 | 734–1235 | 79.7 | 0.06 | 7 of 10 | 295.2 ± 5.4 | 47.6 ± 24.7 |
| UW55D4B | | | | 121 | 0.26 | 51.2 ± 13.9 | 729–1235 | 93.9 | 0.01 | 8 of 10 | 295.7 ± 4.5 | 45.0 ± 24.9 |
| UW55D3B | | | | 124 | 0.26 | 58.9 ± 13.1 | 680–1250 | 72.4 | 0.02 | 6 of 11 | 294.8 ± 9.8 | 47.0 ± 40.1 |
| UW55D4T | | | | 120 | 0.27 | 50.4 ± 14.6 | 670–1220 | 99.6 | 0.08 | 9 of 10 | 296.2 ± 3.6 | 43.4 ± 18.5 |
| UW55D3T | | | | | | Weighted mean plateau age: | | | | 30 of 41 | | |
| <u>SM-05-07</u> | 14 44.857 | 91 34.135 | 2314 | 120 | 0.19 | 75.1 ± 14.2 | 650–1160 | 82.7 | 0.26 | 7 of 10 | 296.2 ± 3.8 | 48.0 ± 31.6 |
| UW53E3 | | | | 120 | 0.19 | 84.1 ± 12.5 | 650–1180 | 77 | 0.12 | 7 of 10 | 295.6 ± 3.0 | 52.7 ± 27.6 |
| UW57E2 | | | | 121 | 0.2 | 77.3 ± 14.3 | 650–1160 | 77.7 | 0.09 | 7 of 10 | 295.4 ± 4.5 | 54.3 ± 35.7 |
| UW57E2B | | | | | | Weighted mean plateau age: | | | | 21 of 30 | | |
| <u>SM-05-06</u> | 14 44.925 | 91 34.016 | 2369 | 122 | 0.21 | 64.6 ± 20.7 | 711–1210 | 66.9 | 0.09 | 5 of 10 | 295.6 ± 7.4 | 60.0 ± 44.5 |
| UW55B1B | | | | 121 | 0.21 | 67.9 ± 34.5 | 704–1200 | 92.9 | 0.31 | 8 of 10 | 295.9 ± 5.5 | 57.8 ± 35.1 |
| UW55B2T | | | | 120 | 0.21 | 66.8 ± 22.0 | 650–1200 | 94.6 | 0.27 | 10 of 12 | 295.8 ± 2.1 | 57.4 ± 17.0 |
| UW55B1T | | | | | | Weighted mean plateau age: | | | | 23 of 32 | | |
| <u>SM-05-05</u> | 14 44.885 | 91 34.017 | 2367 | 120 | 0.19 | 75.4 ± 25.0 | 722–1250 | 79.2 | 0.17 | 7 of 10 | 296.0 ± 4.9 | 66.6 ± 44.0 |
| UW55D2B | | | | 119 | 0.19 | 81.0 ± 31.1 | 717–1220 | 83.9 | 0.01 | 7 of 10 | 295.3 ± 6.5 | 74.0 ± 62.0 |
| UW55D1B | | | | 121 | 0.19 | 70.8 ± 39.9 | 680–1180 | 69.4 | 0.14 | 8 of 10 | 295.9 ± 7.7 | 65.1 ± 66.0 |
| UW55D2T | | | | 121 | 0.19 | 105 ± 28.1 | 670–1220 | 92.1 | 0.07 | 8 of 12 | 296.2 ± 2.4 | 65.7 ± 35.7 |
| UW55D1T | | | | | | Weighted mean plateau age: | | | | 30 of 42 | 296.0 ± 2.0 | 67.0 ± 24.0 |

(continued)

TABLE 2. SUMMARY OF $^{48}\text{Ar}/^{39}\text{Ar}$ INCREMENTAL-HEATING EXPERIMENTS ON GROUNDMASS FROM 15 LAVA FLOWS (continued)

| Sample number Experiment | GPS coordinates (WGS 84 datum) | | Elevation (masl) | Weight (mg) | K/Ca total | Total fusion Age $\pm 2\sigma$ (ka) | Increments used ($^{\circ}\text{C}$) | ^{39}Ar | | Age spectrum | | Isochron analysis | | |
|-----------------------------|--------------------------------|------------------------------|---------------------|----------------|---------------|---|--|------------------|------------------------------------|--------------|----------|-------------------|---------------------------------|---------------------------|
| | Latitude (deg min.ddd N) | Longitude (deg min.ddd W) | | | | | | (%) | Age $\pm 2\sigma$ (ka) | MSWD | N | MSWD | $^{40}\text{Ar}/^{39}\text{Ar}$ | Age $\pm 2\sigma$ (ka) |
| SM-05-04 | 14 44.886 | 91 33.956 | 2372 | | | | | | | | | | | |
| UW55A5B | | | | 127 | 0.18 | 87.4 \pm 29.6 | 683–1220 | 82.5 | 74.0 \pm 21.4 | 0.08 | 7 of 10 | 0.1 | 295.5 \pm 4.2 | 73.8 \pm 68.4 |
| UW55A6T | | | | 123 | 0.17 | 98.3 \pm 27.2 | 679–1220 | 77.9 | 78.2 \pm 19.5 | 0.09 | 6 of 10 | 0.11 | 295.3 \pm 4.6 | 81.9 \pm 71.7 |
| UW55A5T | | | | 122 | 0.18 | 72.3 \pm 26.8 | 670–1220 | 86 | 72.8 \pm 26.2 | 0.05 | 7 of 12 | 0.06 | 295.5 \pm 3.6 | 73.3 \pm 74.4 |
| | | | | | | Weighted mean plateau age: | | | 75.0 \pm 13.0 | 0.07 | 20 of 32 | | | |
| SM-05-02 | 14 44.861 | 91 33.922 | 2347 | | | | | | | | | | | |
| UW55A3B | | | | 139 | 0.18 | 65.2 \pm 18.6 | 717–1210 | 98.8 | 64.5 \pm 15.6 | 0.1 | 9 of 10 | 0.11 | 296.0 \pm 3.5 | 60.3 \pm 31.1 |
| UW55A4B | | | | 122 | 0.17 | 77.7 \pm 24.4 | 723–1223 | 90.3 | 71.6 \pm 17.6 | 0.03 | 8 of 10 | 0.01 | 296.4 \pm 5.2 | 64.6 \pm 42.6 |
| UW55A3T | | | | 118 | 0.17 | 76.4 \pm 24.3 | 640–1220 | 99.2 | 71.1 \pm 13.3 | 0.18 | 11 of 12 | 0.19 | 296.1 \pm 3.4 | 66.3 \pm 28.9 |
| UW55A4T | | | | 122 | 0.18 | 77.0 \pm 17.3 | 680–1200 | 92 | 73.5 \pm 13.2 | 0.02 | 8 of 10 | 0.03 | 295.7 \pm 3.9 | 72.3 \pm 31.0 |
| | | | | | | Weighted mean plateau age: | | | 70.5 \pm 7.3 | 0.27 | 36 of 42 | | | |
| SM-05-01 | 14 45.233 | 91 33.96 | 2400 | | | | | | | | | | | |
| UW55A1B | | | | 122 | 0.17 | 65.5 \pm 25.1 | 632–1180 | 70.7 | 64.7 \pm 22.7 | 0.01 | 6 of 10 | 0.01 | 295.4 \pm 8.0 | 65.5 \pm 85.2 |
| UW55A1T | | | | 124 | 0.18 | 82.1 \pm 24.8 | 680–1250 | 92.2 | 81.5 \pm 19.7 | 0.04 | 6 of 11 | 0.03 | 294.8 \pm 4.8 | 89.2 \pm 56.8 |
| UW55A2T | | | | 123 | 0.2 | 74.6 \pm 26.8 | 620–1110 | 94.5 | 72.0 \pm 16.0 | 0.19 | 7 of 10 | 0.23 | 295.3 \pm 5.4 | 74.4 \pm 54.6 |
| | | | | | | Weighted mean plateau age: | | | 75.0 \pm 11.0 | 0.83 | 19 of 31 | | | |
| SM-07-07 | 14 47.080 | 91 32.947 | 2659 | | | | | | | | | | | |
| UW64D52 | | | | 126 | 0.09 | 81.9 \pm 33.8 | 750–1325 | 88.5 | 92.2 \pm 41.5 | 1.47 | 6 of 7 | 1.73 | 296.2 \pm 2.7 | 73.0 \pm 57.1 |
| UW64H106 | | | | 133 | 0.08 | 121.8 \pm 37.8 | 750–1325 | 97.8 | 114.9 \pm 32.8 | 0.72 | 6 of 7 | 0.80 | 296.3 \pm 2.4 | 84.8 \pm 64.6 |
| UW66A6 | | | | 157 | 93.1 | 88.8 \pm 36.0 | 780–1350 | 93.1 | 99.7 \pm 29.0 | 1.34 | 7 of 7 | 1.23 | 293.9 \pm 2.7 | 130.9 \pm 53.1 |
| | | | | | | Weighted mean plateau age: | | | 103.0 \pm 19.0 | 0.42 | 18 of 21 | | | |
| SM-07-08 | 14 47.070 | 91 32.950 | 2670 | | | | | | | | | | | |
| UW64D56 | | | | 128 | 0.11 | 288.5 | 700–1325 | 100.0 | 248.3 \pm 33.6 | 1.51 | 13 of 13 | 1.12 | 299.1 \pm 3.2 | 156.6 \pm 63.2 |
| UW66B8 | | | | 168 | 0.08 | 231.5 | 800–1300 | 100.0 | 220.1 \pm 28.6 | 1.04 | 8 of 8 | 1.02 | 297.1 \pm 2.9 | 172.5 \pm 77.4 |
| | | | | | | Weighted mean isochron age: | | | 163.0 \pm 49.0 | | 21 of 21 | | 298.0 \pm 2.1 | |

Note: Ages calculated relative to 1,194 \pm 0.012 Ma Alder Creek rhyolite sanidine (Renne et al., 1998), with the exception of four experiments prefixed UW66; for those 28.34 \pm 0.28 Ma Taylor Creek rhyolite sanidine was used. Ages in bold are preferred; see text for discussion. Abbreviations: GPS—global positioning system; MSWD—mean square of weighted deviates.

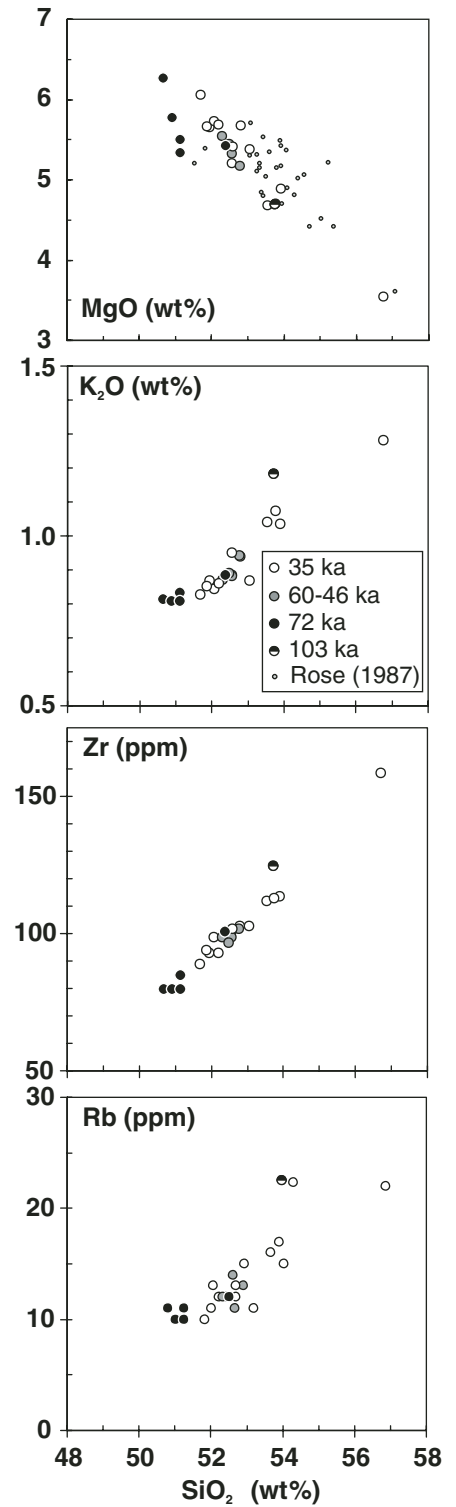


Figure 8. Variation of MgO, K₂O, Zr, and Rb with SiO₂ contents of the Santa María cone-forming lavas. The range in composition (illustrated only for MgO–SiO₂) overlaps the data of Rose et al. (1977) and Rose (1987) from essentially the same set of lava flows, with the exception of the most MgO-rich and SiO₂-poor lavas of phase II (72 ka).

K₂O, 90 ppm Zr, and 11 ppm Rb. In turn, the 60–46 ka lavas of phase III are compositionally uniform and on average higher in SiO₂, K₂O, Zr, and Rb and lower in MgO than the underlying phase II lavas. The final cone-building lavas of phase IV show a greater range, and more scatter, with respect to major and trace element composition, but on average also include the most evolved andesitic lavas of the composite cone (Fig. 8).

Overall, the evolution from basaltic to andesitic magma is not monotonic over time when the crater lavas are considered in stratigraphic context. Rather, the onset of phase IV activity is associated with lavas showing a progressive decrease in SiO₂ and incompatible elements, and a concomitant increase in MgO. These lavas are followed by a group in which SiO₂ and incompatible elements increase, and MgO de-

creases over time. Relative to the earlier phases of cone growth, the latter part of the phase IV lava sequence shows more significant scatter in elemental concentrations, as well as in ratios of highly incompatible trace elements (Fig. 9). This variation is small, however, when the cone-building lavas are considered alongside the subsequent products of the 1902 airfall deposit and the Santiaguito dacite dome. The 1902 deposit is dominated by dacitic pumice (65%–69% SiO₂), but it also contains a small proportion of basaltic andesitic scoria (52%–54% SiO₂) that is remarkably similar to the cone-building lavas of phase IV (Williams and Self, 1983; Rose, 1987). The Santiaguito dome began to grow in 1922, and its lavas contain slightly less SiO₂ (65%), more MgO (1.9%), and less Rb (35 ppm) on average than pumice of the 1902 eruption. A

few of the many lobes of the Santiaguito dome lavas contain fine-grained quenched inclusions of andesitic composition (56%–59% SiO₂) that are also lower in MgO and higher in Rb than the basaltic andesitic scoria of the 1902 eruption (Rose, 1987; Fig. 9).

Volume Estimates

To model the volumetric evolution of the Santa María cone, we consider the shape of the volcanic edifice to be a solid of revolution—an assumption based on its typical composite cone axisymmetrical shape, reflected by the surface topography and the internal structure exposed in the 1902 crater (Figs. 2 and 3). Although some lava flows may have erupted from lateral vents, we assume that the volcano grew

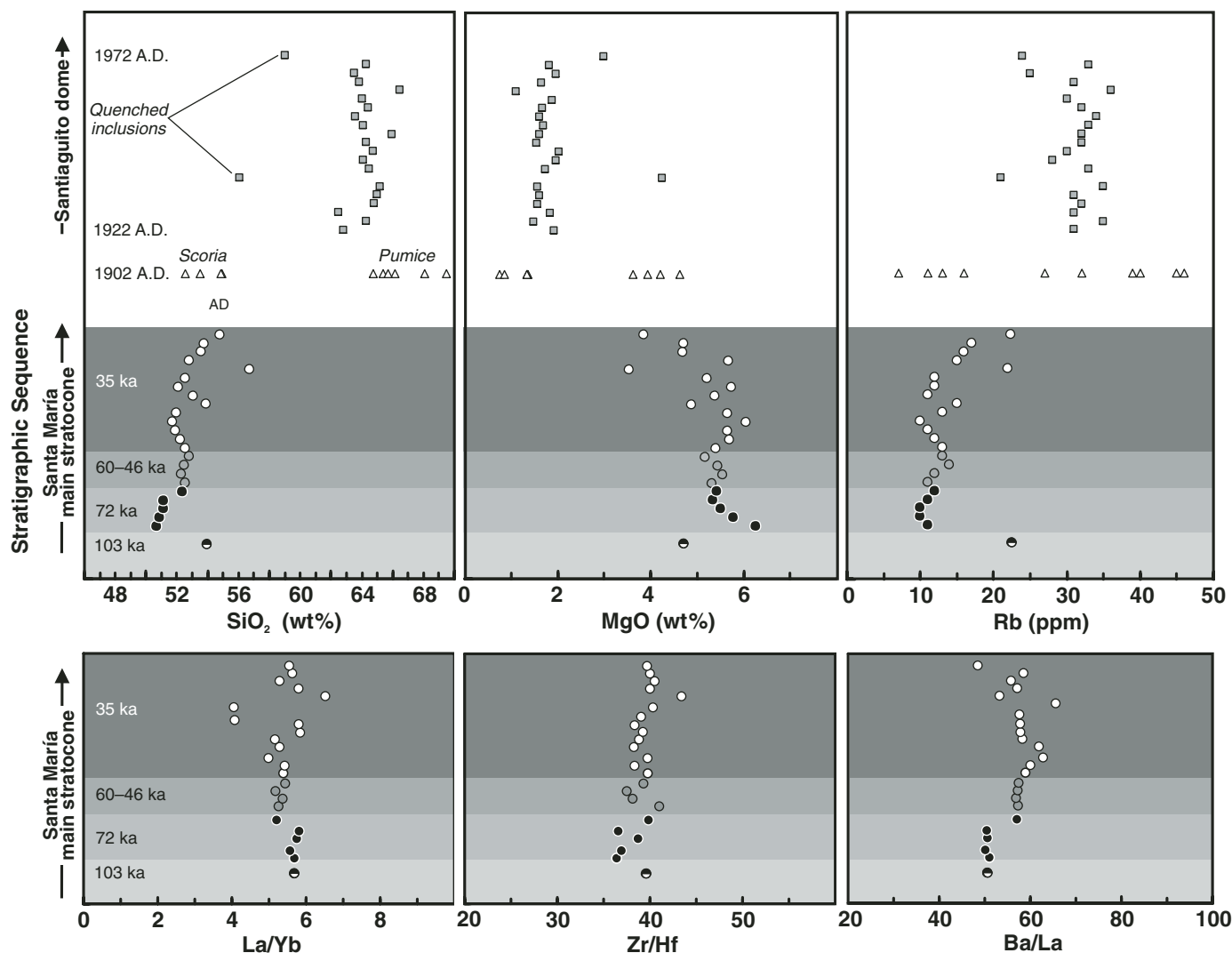


Figure 9. SiO₂, MgO, Rb, La/Yb, Zr/Hf, and Ba/La variation with stratigraphic position. The four phases of main cone growth, shown with different gray backgrounds, preceded the 1902 eruption and the subsequent eruption of lavas comprising the Santiaguito dome between 1922 and 1972. Data and symbols for the main cone lavas as in Figure 8. Data from the 1902 and 1922–1972 A.D. products are from Rose (1972, 1987).

mainly through eruptions from a central vent located on the vertical axis of symmetry, and that this symmetry was maintained throughout its growth. We further assume that the locations of the sampled lavas in Figure 3 each represent the position of the volcanic edifice surface at the time when the corresponding lava flow was emplaced; the volume of the edifice at that time is the volume enclosed by the revolution surface that passes through the sampling site location, and the pre-Santa María basement surface.

Basement topography was estimated using an approach similar to Frey et al. (2004), defining a sloping surface that follows the WNW-trending ridges of the regional topography. The characteristic profile chosen for the revolution surface is a parabolic curve, following the morphologic characterization by Bemis (1995), adapted to a set of profiles obtained from the present-day topography of the edifice. The areal extent of the Santa María cone was calculated using the geologic map of Rose (1987) but ignoring lava flows of unit *Qsmf* that extend far beyond the main cone structure (Fig. 2).

The hypothesis of perfect radial cone growth may be invalidated by many factors, including the preferential emplacement of material along specific sectors of the volcano during different periods of time. To assess the impact that this asymmetry in growth could have in our volume calculations, we considered a simple model in which the vent location at some point in time “shifts” in the opposite direction from the sampling sites, causing the new erupted material to accumulate preferentially in the sector that is in the direction of the shift, and stopping the deposition of material in the sector we sampled. This continues until the cone has grown to an elevation at which the new flank can “engulf” the older cone completely. We found that for a cone of the size and average slope that we inferred for Santa María during the different phases of growth, a permanent vent shift of a few hundreds of meters could represent a missing volume of a few km³.

It is possible that the gaps, and in general the variations in growth rates that we report, are entirely caused by the effect of preferential sector emplacement; however, the assumption that the shift is permanent and in the opposite direction from the summit is an extreme scenario, unlikely to have actually occurred. More likely is the case in which the vent location changed randomly on different occasions, sometimes shedding volcanic material in the direction of the sampled section, and other times emplacing material in other sectors. The lack of any linear trends in vent locations, in contrast to what can be seen at other nearby volcanoes (e.g., Fuego, Acatenango, and Tolimán, Fig. 1), and

the high degree of symmetry of the cone suggest that a randomly directed and ephemeral vent shift is more likely to be the case for Santa María. Our assumption therefore is that the effects of increasing and decreasing the eruptive rate by shifting the deposition of material in sectors around the volcano were averaged out over time to some degree, and these variations are not as severe as to be entirely responsible for the gaps recorded at the sampled section. In the future, more extensive sampling in the 1902 crater (though quite dangerous owing to eruptions from Santiaguito and rockfall from Santa María) could help to resolve this problem.

DISCUSSION

Paleomagnetism, Volcano Evolution, and the Mono Lake Excursion?

The VGPs calculated from the lavas in the crater section define a spatial pattern, including clustering of poles (directions), that is consistent with the ⁴⁰Ar/³⁹Ar age determinations and unconformable breaks in the stratigraphy. For example, the lava flows of cone-building phase II, dated at 72 ± 5 ka yield VGPs clustered near the Earth’s rotation axis, whereas the next youngest lavas of phase III, dated between 60 and 46 ka, have VGPs tightly clustered over northern Scandinavia (Fig. 6A), consistent with secular variation and a temporal gap in the section (Fig. 3B). The 12 lava flows of cone-building phase IV, dated at 35 ± 2 ka, reveal a far more complex pattern that begins with four VGPs clustered in a position over Scandinavia that is similar to that of the underlying phase III lavas; the next four VGPs are located farther east and southward down to 60° N latitude; these are followed by a 43° shift westward to a single VGP over northeastern Canada, then a move back east to a cluster of four VGPs over the North Atlantic Ocean (Fig. 6A). The difference in VGPs (paleomagnetic directions) confirms that the lavas of cone-building phases II and III are temporally distinct, as evinced by the stratigraphy and ⁴⁰Ar/³⁹Ar ages (Fig. 5). In contrast, the VGPs of phase IV lavas record a brief period of high-amplitude secular variation, ultimately resulting in a cluster of VGPs over the North Atlantic Ocean.

Based on additional measurements from oriented block samples and reanalysis of paleomagnetic data collected by Rose et al. (1977), Conway et al. (1994) suggested the lava flows in the crater section preserve a record of the Mono Lake excursion that was best constrained at that time by ¹⁴C dating to ~28–25 ka. The similarity of several VGPs over northeastern Canada and the North Atlantic Ocean indicates that the short lava section studied by Conway et al.

(1994) corresponds closely with the phase IV lavas at the top of the crater section (Fig. 6A). Notably, the Conway et al. (1994) section includes more flow sites (4C to 8C) that record VGPs over Canada than the single site (flow 18) in the crater section (Fig. 6A). The Mono Lake excursion was originally documented in Wilson Creek Formation sediments by Denham and Cox (1971) as a large counterclockwise loop of VGPs over North America. Later work by Liddicoat and Coe (1979) on additional sites in the Wilson Creek Formation revealed that an even larger clockwise looping of VGPs over Eurasia preceded the loop found by Denham and Cox (1971). More recently, Channell (2006) discovered the Mono Lake excursion in ODP site 919 sediments south of Iceland; the VGPs loop in a counterclockwise direction to the equator over the Pacific Ocean (Fig. 6B).

The inclination waveform found in the Santa María crater section, including a shift from 35° at the bottom of the section to -12.0° in the middle, with a shift to >57°, before reaching 33.3° at the top (Fig. 5), is similar to that of the Mono Lake excursion. This “waveform” was the feature interpreted first by Rose et al. (1977) as a geomagnetic excursion and later by Conway et al. (1994) as the Mono Lake excursion. However, the declination pattern shows little correlation to that found in the Wilson Creek sediments. Moreover, we now know that only the uppermost part of the crater section, the phase IV lavas that have been ⁴⁰Ar/³⁹Ar dated at 35 ± 2 ka, correspond in time with the Mono Lake excursion, which recently has been astrochronologically and radioisotopically dated at 32–34 ka (Channell, 2006; Laj and Channell, 2007; Cassata et al., 2008).

Although the 35 ± 2 ka phase IV lavas record a brief period of enhanced secular variation, the lack of VGPs extending below 60° N latitude argues that these lavas do not clearly record the Mono Lake excursion (Fig. 6B). Alternatively, the absence of clearly excursive VGPs may reflect incomplete sampling of the paleofield by the 12 phase IV lava flows exposed in the 1902 crater wall. Paleointensity measurements of these lavas would presumably shed light on whether the prominent, but very brief, ca. 1.5 ka, intensity minimum associated with the Mono Lake excursion in global marine sediments (Laj et al., 2004) is partly captured at Santa María.

Eruptive Rates and Tectonic Setting

We estimate that the total volume of the Santa María composite cone (prior to the 1902 eruption) is ~8 km³. Together with the ⁴⁰Ar/³⁹Ar ages, our volume calculations imply a four-phase history of cone growth (Fig. 10A). Initially,

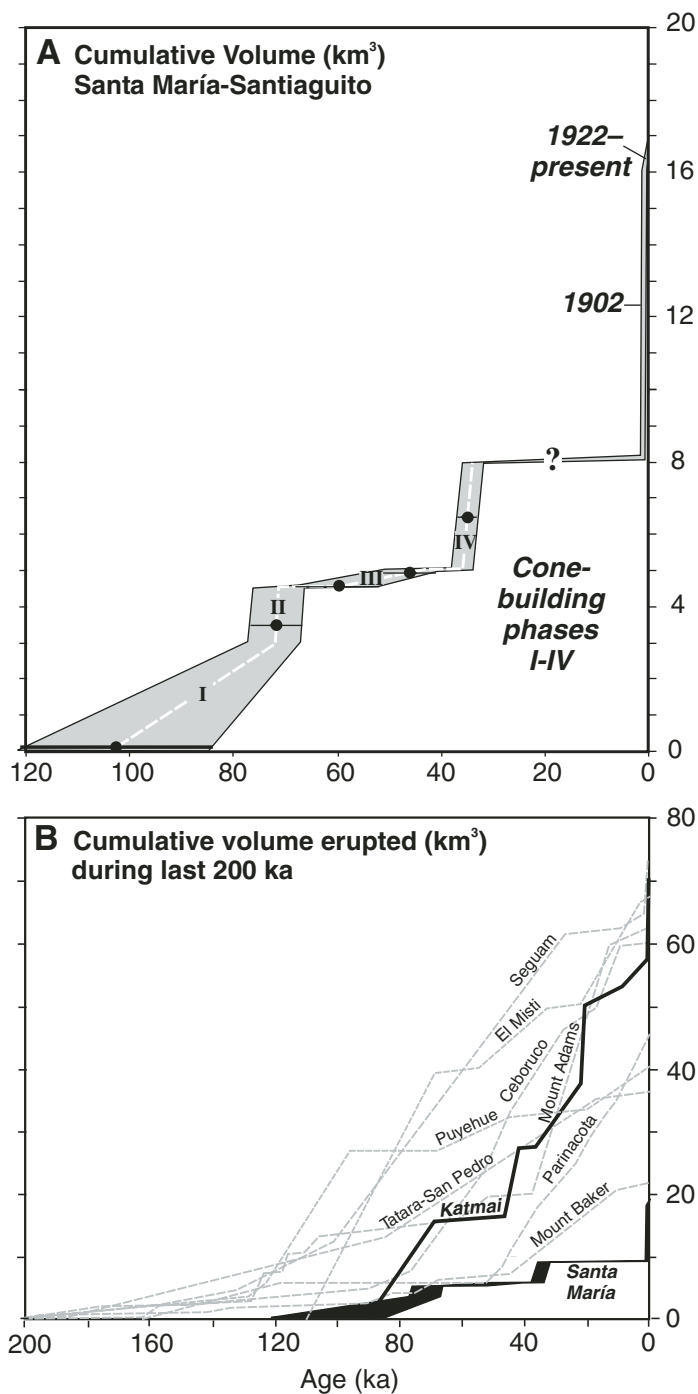


Figure 10. Cumulative growth of Volcán de Santa María over time. (A) The eruptive activity of cone building has been subdivided into four phases based on the stratigraphy (Fig. 3A) and ⁴⁰Ar/³⁹Ar ages (Table 2). Although there are peaks of activity during cone-building phases II and IV, the largest contribution to the erupted volume is the 1902 plinian eruption. Note the exaggerated duration of the 1902 eruption along the age axis for illustrative purposes only. (B) Comparison of Volcán de Santa María to other long-lived, well-dated frontal arc composite volcanoes. Growth curves extracted from data in: Hildreth and Lanphere (1994, Mount Adams), Singer et al. (1997, Tatara San Pedro; 2008, Puyehue), Jicha and Singer (2006, Seguam), Thouret et al., (2001, El Misti), Hildreth and Lanphere (1994, Mount Adams; 2003b, Mount Baker), Frey et al. (2004, Ceboruco), Hora et al. (2007, Parímacota). The heavy curve for the Katmai cone from Hildreth et al. (2003a) illustrates the contrast between volcanoes that rank first and second in the scale of their twentieth-century eruptions.

~3 km³ was erupted between 103 and 72 ka, ~1.5 km³ was added at 72 ka, <1 km³ erupted between ~60 and 46 ka, and a final pulse of growth encompassing ~3.3 km³ occurred at ca. 35 ka. There is no evidence of further volcanic activity until the 8 km³ plinian eruption of dacite in 1902. Lack of age determinations from the oldest phase I of cone growth clearly limits our understanding, but the simplest hypothesis is that growth during this period of ca. 30 ka was linear (Fig. 10A).

The average eruptive rate for the 68 ka cone-building period between 103 and 35 ka is 0.12 km³/ka; a rate of 0.16 km³/ky is obtained, if the time period is extended to the present and the products of the 1902 eruption and the Santiaguito dome are included. Age uncertainties overlap for the individual lava flows within the 72 and 35 ka packages that define phases II and IV, suggesting that emplacement of individual flow units and perhaps entire lava packages may have occurred rapidly (a few centuries or less). From the previous reasoning and from analogies with other recently active volcanoes in the region (Fuego and Pacaya), the peak rates could be an order of magnitude higher (~1 km³/ka) during these periods of intense activity (Fig. 10A). Although the estimates of eruption rate are sensitive to uncertainties of the age determinations, the impact on the average long-term rate is relatively small. For example, considering the extrema of the uncertainty in the age determinations, rather than the mean ages, could shift our long term average by ±25%.

Despite the size of the 1902 dacite eruption, the average long-term eruptive rate of 0.1–0.2 km³/ka at Santa María–Santiago is remarkably low relative to other well-dated arc volcanoes (Fig. 10B; White et al. 2006; Singer et al., 2008). For instance White et al. (2006) presented a compilation of 34 eruption rates for continental and oceanic arc volcanoes, covering a range from 0.02 to 27 km³/ka with a mean value of 2.3 km³/ka. Moreover, the rate is low compared to the very rough estimates for other composite volcanoes including Fuego (2.4 km³/ka over the past 17 ka), Pacaya (~1 km³/ka), and Atitlán (>0.4 km³/ka over up to 84 ka) along the Central American volcanic arc (Conway et al., 1994; Carr et al., 2003). It should be noted that these rates are based on extrapolations from relatively short periods of record and are not constrained by radioisotopic dating. The low long-term growth rate at Santa María may reflect differences in tectonic setting and stress field along the Central American volcanic arc (White et al., 2006), with Santa María being located atop the thickest crust in a region that has experienced less extension relative to other nearby volcanoes. For example, Burkart and

Self (1985) suggest that the large volume of magma erupted in the Atilán volcanic complex (Fig. 2), including 33, 18, and 27 km³ each at the Atilán, Tolimán, and San Pedro composite volcanoes, which all postdate the underlying 84 ka Atilán caldera and the associated 250 km³ Los Chocoyos ignimbrite, reflects regional crustal extension. Farther south, Cameron et al. (2002) infer that extension along the Guatemala City graben promoted decompression melting and enhanced magma production beneath the 17 km³ composite cone of Pacaya volcano.

Magmatic Evolution

The new chronostratigraphy establishes a temporal framework in which we may now interpret changes in erupted magma during the past 103 ka. The new geochemical data support earlier models developed for Santa María (Rose et al., 1977; Rose, 1987); however, our results indicate more compositional overlap between the three later phases of cone building, and possibly more of a continuum of differentiation, than suggested by Rose (1987). The 103 ka phase I lava falls compositionally within the range observed for the much younger 35 ka lavas of cone-building phase IV (Fig. 8), thus there is a reversal in composition and a gap separating the earliest phase of cone-building magma from that of phase II (Fig. 9). The somewhat steady increase in SiO₂, decrease in MgO, and increase in incompatible trace element contents during the period of cone growth between 72 and 35 ka is not monotonic, but rather a slight reversal to more primitive, MgO-rich, SiO₂, and incompatible element-poor, composition characterizes the onset of phase IV lavas (Fig. 9). The compositional reversal indicates that steady fractional crystallization of a single basaltic parent magma between 72 and 35 ka cannot explain the observed evolution of magma composition over time. Moreover, the phase IV lavas that erupted 35 ka show significant scatter in major and trace element abundances, and in ratios of La/Yb, Zr/Hf, and Ba/La which are normally unaffected by crystallization of the observed phenocryst phases, such that crystal fractionation alone cannot explain the differentiation. Presumably mixing between relatively primitive and evolved (andesitic?) magma during this phase of cone growth at 35 ka, is responsible for the scatter as well as reversely zoned phenocrysts common in these lavas (Rose, 1987).

We interpret the major and trace element evolution during cone growth illustrated in Figure 9 to reflect successive batches of basalt erupting after variable degrees of fractionation and minor mixing. This would suggest that no large, long-lived magma reservoir formed beneath the

cone during its growth between 103 and 35 ka. A remarkably similar pattern is preserved geochemically in basaltic to basaltic-andesitic lavas erupted at the Fuego volcanic complex, 80 km east of Santa María (Fig. 1) during the past several thousand years. Chesner and Rose (1984) interpret secular trends in magma composition erupted at Fuego to reflect repeated ascent of basalt out of the lower crust into shallower parts of the plumbing system, wherein the degree of cooling, and hence fractional crystallization, drives differentiation of each magma batch to greater or lesser extent.

Generation of the large volume of 1902 dacite magma by a process of crystal fractionation from a mafic parent magma has been proposed by Rose (1972), Rose et al. (1977), and Williams and Self (1983). The eruption of dacite marks a profound change from a plumbing system in which magma efficiently and frequently ascends and erupts during cone building, to one of stagnation, incubation, and accumulation in the middle to lower crust. Rose et al. (1977) hypothesized that once the cone reached an elevation >3500 masl, ascent of basalt from the deep crust was impeded owing to lithostatic pressure becoming greater than hydrostatic pressure in the deep magma source.

Linking trace element and radiogenic isotope data from the now well-dated sequence of cone-forming lavas, with products of the 1902 A.D. plinian eruption, and subsequent dacitic domes (Fig. 9), is the focus of ongoing work aimed at determining what occurred beneath Santa María during the 35 ka period of repose.

Analogies with Other Volcanoes and Hazard Assessment

From the perspective of hazards, catastrophic silicic eruptions like that which occurred at Santa María in 1902 are clearly a possibility that needs to be considered at other basaltic-andesitic composite volcanoes along the Central American volcanic arc (Fig. 1). Several active composite volcanoes in Guatemala, including Santa María and Fuego, exhibit remarkably similar styles of both physical and geochemical evolution over tens of thousands of years of cone building. These common characteristics include recurrent episodes of small- to moderate-size explosive and effusive activity producing a large proportion of fragmental pyroclastic material and a relatively small volume of lava flows originating at central vents (e.g., Fig. 3C; Vallance et al., 2001; Lyons et al., 2007), as well as repeated ascent and crystal fractionation of basaltic to basaltic-andesitic magma. The 35 ka period of dormancy between the termination of cone building and the 1902 plinian eruption at Santa María is omi-

nous and stands as a reminder that long repose periods tend to be followed by larger and potentially more destructive eruptions (Simkin and Siebert, 2000). Two distinct patterns of volcanic activity can therefore be recognized in relation to the volcanic hazards associated with this kind of volcano: (1) a pattern of frequent, small-volume eruption, associated with the constructive stage of cone building, and (2) a pattern of long dormancy followed by large silicic explosive eruptions, associated with the destruction of the volcanic edifice. In the first case, the hazards associated with explosive eruptions tend to be restricted to areas close to the volcano (e.g., the case of the eruptions of Volcán de Fuego during the past five centuries), and the eruptions that generate them should be expected to occur on a relatively short timescale. In the second case, the hazards associated with explosive eruptions can spread over a much larger area (e.g., the 1902 Santa María eruption), and the eruptions that generate them should be expected to occur only on a very long time scale. In this context, it is important to know when a volcanic plumbing system is shifting from its cone-building stage to one in which magma does not erupt, but rather stagnates, ponds, and undergoes extraordinary degrees of differentiation for several millennia, increasing the potential to produce a large-volume explosive eruption.

Santa María is among the smallest of the composite cones that dominate the frontal arc in the northern segment of the Central American volcanic arc; so clearly, the total eruptive volume of the cone is not a good gage for the potential occurrence of a large explosive eruption. Moreover, the ⁴⁰Ar/³⁹Ar-based age model for Santa María indicates a low eruptive rate for >100 ka, so neither is sustained high output a measure of the hazard of large eruptions. Unfortunately, the absence of ⁴⁰Ar/³⁹Ar-based age constraints similar to those reported here renders it difficult, if not impossible, to determine whether or not other composite volcanoes along the northern segment of the Central American volcanic arc (Fig. 1) have experienced, or are currently experiencing, a long-term decline in eruption rate that could foreshadow the repose which may be required to generate large quantities of gas-rich dacite. The neighboring volcanic systems of Site Orejas and Almolonga-Cerro Quemado have experienced a similar history of erupting progressively more silicic lavas during the main cone-building phase, subsequently undergoing catastrophic cone destruction by a large silicic eruption (Johns, 1975; Gierzycki, 1976). The possibility of a large silicic eruption at any of the composite cones less active historically than Fuego, including Tacaná, Siete Orejas-Chicabal, Atilán, Acatenango, Agua,

Tajumulco, Tolimán, and San Pedro (Fig. 1), deserves attention, especially in the event that any of these volcanoes starts to show signs of unrest, even in the absence of evidence that large explosive eruptions have occurred in the past.

CONCLUSIONS

The geochronologic and paleomagnetic results reveal that Santa María evolved in at least seven stages, including four discrete phases of cone building, a 35 ka period of repose, the 1902 eruption, and growth of the Santiaguito dome complex from 1922 to the present day. Volcanic activity since 103 ka has been highly episodic, displaying a wide variety of eruptive styles and chemical compositions. This is reflected in distinct paleomagnetic, geochronologic, and geochemical characteristics of successive lava packages that comprise the cone. The history from 103 ka to 1902 A.D. was constructional, comprising an initial cone-building phase from 103 to 72 ka (3 km³), phase II at 72 ± 5 ka (1.5 km³), phase III between 60 and 46 ka (<1 km³), and phase IV at 35 ± 2 ka. The cone was built at an average eruption rate of 0.12 km³/ka. Although during the peak phases II and IV, Santa María may have grown at >1 km³/ka, the average growth rate is much lower than for other arc volcanoes, including several along the Central American volcanic arc. In part, the relatively thick crust and compressive stress regime beneath Santa María may play a role in limiting the eruptive output.

The paleomagnetic record captured by lava flows at Santa María shows no clearly excursive directions. However, the youngest phase IV lavas, ⁴⁰Ar/³⁹Ar dated at 35 ± 2 ka, preserve a record of unusually large paleosecular variation over a very short period. This may reflect a subdued response to the brief geodynamo instability associated with the Mono Lake excursion that recently has been astrochronologically and radioisotopically dated at 32–34 ka.

New geochemical data support earlier models developed for both Santa María (Rose et al., 1977; Rose, 1987) and Fuego (Chesner and Rose, 1984) in which these volcanoes are envisioned to have grown through repeated ascent of parental basalt from the deep crust, each batch of which crystallized and evolved to greater or lesser degree toward andesitic compositions. The final phase of rapid cone growth at Santa María, now precisely dated at 35 ± 2 ka, may have inhibited further ascent of basalt from the deep crust, and instead promoted an exceptionally protracted process of accumulation, cooling, and perhaps extensive fractionation of basaltic magma that created the volatile-rich, highly explosive dacite that

erupted in 1902. Testing this hypothesis is the focus of our ongoing research.

The large proportion of pyroclastic material intercalated with a relatively small volume of lava that characterizes Santa María cone building reflects recurrent episodes of small to moderate explosive and effusive eruptive activity, producing hot rockfall, block and ash flow, and lava flow deposits on the steep flanks, in a similar way as has been observed recently at Fuego (Vallance et al., 2001; Lyons et al., 2007). Other neighboring composite volcanoes show a broadly similar history of progressively erupting more silicic magma during the cone growth, followed by catastrophic cone destruction associated with silicic eruptions (Johns, 1975; Gierzycki, 1976). This common mechanism of cone growth and lava composition change through time suggests that Santa María's long evolutionary history may be a good analog for what is possible in the future at other dominantly basaltic-andesitic composite cones in Guatemala that are either historically inactive, or whose central vent activity has waned significantly during historical time. ⁴⁰Ar/³⁹Ar geochronology offers important insight on rates of composite cone growth, and the duration of periods of reduced output or dormancy, that may be useful in a comparative assessment of hazards along the Central American volcanic arc in Guatemala.

ACKNOWLEDGMENTS

Xifan Zhang trained R.P.E.W. in the University of Wisconsin–Madison Rare Gas Geochronology Laboratory, and Sarah Greene assisted in acquiring argon data from samples not in the crater wall. Ingrid Fedde, York Lewis, and Walt Rathbun helped with sample preparation and measurement of remnant magnetization directions. Tom Vogel, David Szymanski, and the staff at the XRF and ICP-MS facilities at Michigan State University provided the geochemical analysis. Nick Rogers kindly provided geochemical data from the Open University. Raul Salguero, Pablo Catalan, Luis A. de la Vega, York Lewis, Jennifer Garrison, Pedro Perez, Sarah Greene, and others helped with the sampling. Brian Jicha's comments helped improve the manuscript. Fieldwork support and digital elevation model and cartography for the Santa María area were provided to R.P.E.W. by the Coordinadora Nacional para la Reducción de Desastres (CONRED–Guatemala). Reviews by S. de Silva, C. Connor, and T. Fischer improved this paper. This research was possible thanks to support from the U.S. National Science Foundation, grants EAR-0337667, EAR-0439155, EAR-0516760, and EAR-0738007.

REFERENCES CITED

Bacon, C.R., and Lanphere, M.A., 2006, Eruptive history and geochronology of Mount Mazama and the Crater Lake region, Oregon: *Geological Society of America Bulletin*, v. 118, p. 1331–1359, doi: 10.1130/B25906.1.
Bemis, K.G., 1995, A Morphometric Study of Volcanoes in Guatemala, Iceland, the Snake River Plain, and the South Pacific [Ph.D. thesis]: Rutgers, The State University of New Jersey, 254 p.

Benson, L., Liddicoat, J., Smoot, J., Sama-Wojcicki, A., Negrini, R., and Lund, S., 2003, Age of the Mono Lake excursion and associated tephra: *Quaternary Science Reviews*, v. 22, p. 135–140, doi: 10.1016/S0277-3791(02)00249-4.
Bhalla, M.S., Kotlia, B.S., and Subrahmanyam, K., 1998, Magnetostratigraphy of fluviolacustrine sediments from Pithoragarh area, Uttar Pradesh: *Journal of the Geological Society of India*, v. 5, p. 167–170.
Burkart, B., and Self, S., 1985, Extension and rotation of crustal blocks in northern Central America and effect on the volcanic arc: *Geology*, v. 13, p. 22–26, doi: 10.1130/0091-7613(1985)13<22:EAROCB>2.0.CO;2.
Cameron, B.I., Walker, J.A., Carr, M.J., Patino, L.C., Matias, O., and Feigenson, M.D., 2002, Flux versus decompression melting at stratovolcanoes in southeastern Guatemala: *Journal of Volcanology and Geothermal Research*, v. 119, p. 21–50, doi: 10.1016/S0377-0273(02)00304-9.
Carr, M.J., and Pontier, N.K., 1981, Evolution of a young parasitic cone towards a mature central vent; Izalco and Santa Ana volcanoes in El Salvador, Central America: *Journal of Volcanology and Geothermal Research*, v. 11, p. 277–292, doi: 10.1016/0377-0273(81)90027-5.
Carr, M.J., Feigenson, M.D., Patino, L.C., and Walker, J.A., 2003, Volcanism and geochemistry in Central America: Progress and problems, in Eiler, J., et al., eds., *Inside the Subduction Factory: American Geophysical Union, Geophysical Monograph 138*, p. 153–179.
Cassata, W.S., Singer, B.S., and Cassidy, J., 2008, Laschamp and Mono Lake geomagnetic excursions recorded in New Zealand: *Earth and Planetary Science Letters*, v. 268, p. 76–88, doi: 10.1016/j.epsl.2008.01.009.
Channell, J.E.T., 2006, Late Brunhes polarity excursions (Mono Lake, Laschamp, Iceland Basin and Pringle Falls) recorded at ODP Site 919 (Irminger Basin): *Earth and Planetary Science Letters*, v. 244, p. 378–393, doi: 10.1016/j.epsl.2006.01.021.
Chesner, C.A., and Rose, W.I., 1984, Geochemistry and evolution of the Fuego volcanic complex, Guatemala: *Journal of Volcanology and Geothermal Research*, v. 21, p. 25–44, doi: 10.1016/0377-0273(84)90014-3.
Conway, F.M., Vallance, J.W., Rose, W.I., Johns, G.W., and Paniagua, S., 1992, Cerro Quemado, Guatemala: The volcanic history and hazards of an exogenous volcanic dome complex: *Journal of Volcanology and Geothermal Research*, v. 52, p. 303–323, doi: 10.1016/0377-0273(92)90051-E.
Conway, F.M., Diehl, J.F., Rose, W.I., and Matias, O., 1994, Age and magma flux of Santa María Volcano, Guatemala: Correlation of paleomagnetic waveforms with the 28,000 to 25,000 yr B.P. Mono Lake Excursion: *The Journal of Geology*, v. 102, p. 11–24.
Davidson, J., and De Silva, S., 2000, Composite volcanoes, in Sigurdsson, H., *Encyclopedia of Volcanoes*: Academic Press, p. 663–681.
Denham, C.R., and Cox, A., 1971, Evidence that the Laschamp polarity event did not occur 13,300–30,400 years ago: *Earth and Planetary Science Letters*, v. 13, p. 181–190, doi: 10.1016/0012-821X(71)90122-1.
Durst, K.S., 2008, Erupted Magma Volume Estimates at Santiaguito and Pacaya Volcanoes, Guatemala Using Digital Elevation Models [M.S. thesis]: Houghton, Michigan Technological University, 38 p.
Fisher, R.A., 1953, *Dispersion on a sphere*: London, *Proceeding of the Royal Society, Series A*, v. 217, p. 295–305.
Frey, H.M., Lange, R.A., Hall, C.M., and Delgado-Granados, H., 2004, Magma eruption rates constrained by ⁴⁰Ar/³⁹Ar chronology and GIS for the Ceboruco–San Pedro volcanic field, western Mexico: *Geological Society of America Bulletin*, v. 116, p. 259–276, doi: 10.1130/B25321.1.
Gamble, J.A., Price, R.C., Smith, I.E.M., McIntosh, W.C., and Dunbar, N.W., 2003, ⁴⁰Ar/³⁹Ar geochronology of magmatic activity, magma flux and hazards at Ruapehu volcano, Taupo Volcanic Zone, New Zealand: *Journal of Volcanology and Geothermal Research*, v. 120, p. 271–287, doi: 10.1016/S0377-0273(02)00407-9.
Gierzycki, G.A., 1976, *Geology and geochemistry of three andesitic stratovolcanoes, Colomb quadrangle,*

- Guatemala [M.S. thesis]: Houghton, Michigan Technological University, 86 p.
- Haapala, J.M., Escobar Wolf, R., Vallance, J.W., Rose, W.I., Griswold, J.P., Schilling, S.P., Ewert, J.W., and Mota, M., 2005, Volcanic hazards at Atitlán Volcano, Guatemala: U.S. Geological Survey Open-File Report, 2005-1403.
- Hagstrum, J.T., and Champion, D.E., 1995, Late Quaternary geomagnetic secular variation from historical and ^{14}C -dated lava flows on Hawaii: *Journal of Geophysical Research*, v. 100, p. 24,393–24,403, doi: 10.1029/95JB02913.
- Halsor, S.P., and Rose, W.I., 1988, Common characteristics of paired volcanoes in northern Central America: *Journal of Geophysical Research*, v. 93, p. 4467–4476, doi: 10.1029/JB093iB05p04467.
- Harris, A.J., Rose, W.I., and Flynn, L.P., 2003, Temporal trends in lava dome extrusion at Santiaguito 1922–2000: *Bulletin of Volcanology*, v. 65, p. 77–89.
- Hildreth, W., and Lanphere, M.A., 1994, Potassium-argon geochronology of a basalt-andesite-dacite arc system: The Mount Adams volcanic field, Cascade Range of southern Washington: *Geological Society of America Bulletin*, v. 106, p. 1413–1429, doi: 10.1130/0016-7606(1994)106<1413:PAGOAB>2.3.CO;2.
- Hildreth, W., Lanphere, M.A., and Fierstein, J., 2003a, Geochronology and eruptive history of the Katmai volcanic cluster, Alaska Peninsula: *Earth and Planetary Science Letters*, v. 214, p. 93–114, doi: 10.1016/S0012-821X(03)00321-2.
- Hildreth, W., Fierstein, J., and Lanphere, M.A., 2003b, Eruptive history and geochronology of the Mount Baker volcanic field, Washington: *Geological Society of America Bulletin*, v. 115, p. 729–764, doi: 10.1130/0016-7606(2003)115<0729:EHAGOT>2.0.CO;2.
- Hora, J.M., Singer, B.S., and Wörner, G., 2007, Volcano evolution and eruptive flux on the thick crust of the Andean Central volcanic zone: $^{40}\text{Ar}/^{39}\text{Ar}$ constraints from Volcán Parímacota, Chile: *Geological Society of America Bulletin*, v. 119, p. 343–362, doi: 10.1130/B25954.1.
- Jicha, B.R., and Singer, B.S., 2006, Volcanic history and magmatic evolution of Segum Island, Aleutian Island arc, Alaska: *Geological Society of America Bulletin*, v. 118, p. 805–822, doi: 10.1130/B25861.1.
- Johns, G.W., 1975, Geology of the Cerro Quemado volcanic dome complex, Guatemala [M.S. thesis]: Houghton, Michigan Technological University, 124 p.
- Kent, D.V., Hemming, S.R., and Turrin, B.D., 2002, Laschamp excursion at Mono Lake?: *Earth and Planetary Science Letters*, v. 197, p. 151–164, doi: 10.1016/S0012-821X(02)00474-0.
- Kirschvink, J.L., 1980, The least-squares line and plane and the analysis of paleomagnetic data: *Geophysical Journal of the Royal Astronomical Society*, v. 62, p. 699–718.
- Kotlia, B.S., Bhalla, M.S., Sharma, C., Rajagopalan, G., Ramesh, R., Chauhan, M.S., Mather, P.D., Bhandari, S., and Chacko, T., 1997, Paleoclimatic conditions in the upper Pleistocene and Holocene Bhimtal-Naukuchiatal lake basin in south-central Kumaun, North India: *Palaeogeography, Palaeoclimatology, Palaeoecology*, v. 130, p. 307–322, doi: 10.1016/S0031-0182(96)00126-5.
- Laj, C., and Channell, J.E.T., 2007, Geomagnetic excursions, *in* Kono, M. ed., *Treatise in Geophysics: Volume 5, Geomagnetism*: Amsterdam, Elsevier, *Encyclopedia of Geophysics*, chap. 10, p. 373–416.
- Laj, C., Kissel, C., and Beer, J., 2004, High resolution global paleointensity stack since 75 ka (GLOPIS-75) calibrated to absolute values, *in* Channell, J.E.T., et al., eds., *Timescales of the Paleomagnetic Field*: American Geophysical Union, *Monograph Series*, v. 145, p. 255–265.
- Levi, S., and Karlin, A., 1989, A sixty thousand year paleomagnetic record from the Gulf of California sediments: Secular variation, late quaternary excursions, and geomagnetic implications: *Earth and Planetary Science Letters*, v. 92, p. 219–233, doi: 10.1016/0012-821X(89)90048-4.
- Liddicoat, J.C., 1992, Mono Lake excursion in the Mono Basin, California, and at Carson sink and Pyramid Lake, Nevada: *Geophysical Journal International*, v. 108, p. 442–452, doi: 10.1111/j.1365-246X.1992.tb04627.x.
- Liddicoat, J.C., 1996, Mono Lake excursion in the Lahontan Basin, Nevada: *Geophysical Journal International*, v. 125, p. 630–635, doi: 10.1111/j.1365-246X.1996.tb00025.x.
- Liddicoat, J.C., and Coe, R.S., 1979, Mono Lake geomagnetic excursion: *Journal of Geophysical Research*, v. 84, p. 261–271, doi: 10.1029/JB084iB01p00261.
- Liddicoat, J.C., Lajoie, K.R., and Sarna-Wojcicki, A.M., 1982, Detection and dating the Mono Lake excursion in the Lake Lahontan Seho Formation, Carson Sink, Nevada: *Eos (Transactions, American Geophysical Union)*, v. 63, p. 920.
- Ligorria, J.P., and Molina, E., 1997, Crustal velocity structure of southern Guatemala using refracted and Sp converted waves: *Geofísica Internacional*, v. 36, p. 9–19.
- Lund, S.P., Liddicoat, J.C., Lajoie, K.R., Henyey, T.L., and Robinson, S.W., 1988, Paleomagnetic evidence for Long-Term (10^4 year) memory and periodic behavior in the earth's core dynamo process: *Geophysical Research Letters*, v. 15, p. 1101–1104, doi: 10.1029/GL015i010p01101.
- Lyons, J.J., Johnson, J.B., Waite, G.P., and Rose, W.I., 2007, Observations of cyclic Strombolian eruptive behavior at Fuego volcano, Guatemala reflected in the seismo-acoustic record: *Eos (Transactions, American Geophysical Union)*, Fall Meeting abstract, V11C-0745.
- Mankinen, E., and Wentworth, C.M., 2004, Mono Lake excursion recorded in sediments of the Santa Clara Valley, California: *Geochemistry Geophysics Geosystems*, v. 5, p. Q02H05, doi: 10.1029/2003GC000592.
- Marco, S., 2002, Late Pleistocene paleomagnetic secular variation from the Sea of Galilee, Israel: *Geophysical Research Letters*, v. 29, no. 21, p. 2015, doi: 10.1029/2001GL014038.
- Martin, D.P., and Rose, W.I., 1981, Behavior patterns of Fuego Volcano, Guatemala: *Journal of Volcanology and Geothermal Research*, v. 10, p. 67–81, doi: 10.1016/0377-0273(81)90055-X.
- McFadden, P.L., and McElhinny, M.W., 1988, The combined analysis of remagnetization circles and direct observation in paleomagnetism: *Earth and Planetary Science Letters*, v. 87, p. 161–172, doi: 10.1016/0012-821X(88)90072-6.
- Negrini, R.M., Davis, J.O., and Verosub, K.L., 1984, Mono Lake geomagnetic excursion found at Summer Lake, Oregon: *Geology*, v. 12, p. 643–646, doi: 10.1130/0091-7613(1984)12<643:MLGEFA>2.0.CO;2.
- Nowaczyk, N.R., 1997, High-resolution magnetostratigraphy of four sediment cores from the Greenland Sea—II. Rock magnetic and relative paleointensity data: *Geophysical Journal International*, v. 131, p. 325–354, doi: 10.1111/j.1365-246X.1997.tb01225.x.
- Nowaczyk, N.R., and Antonow, M., 1997, High-resolution magnetostratigraphy of four sediment cores from the Greenland Sea—II. Rock magnetic and relative paleointensity data: *Geophysical Journal International*, v. 131, p. 310–324, doi: 10.1111/j.1365-246X.1997.tb01224.x.
- Nowaczyk, N.R., and Knies, J., 2000, Magnetostratigraphic results from the eastern Arctic Ocean: AMS ^{14}C ages and relative paleointensity data of the Mono Lake and Laschamp geomagnetic reversal excursions: *Geophysical Journal International*, v. 140, p. 185–197, doi: 10.1046/j.1365-246x.2000.00001.x.
- Rebollar, C.J., Espindola, V.H., Uribe, A., Mendoza, A., and Pérez-Verti, A., 1999, Distribution of stress and geometry of the Wadati-Benioff zone under Chiapas, Mexico: *Geofísica Internacional*, v. 38, p. 95–106.
- Renne, P.R., Swisher, C.C., Deino, A.L., Karner, D.B., Owens, T.L., and DePaolo, D.J., 1998, Intercalibration of standards, absolute ages and uncertainties in $^{40}\text{Ar}/^{39}\text{Ar}$ dating: *Chemical Geology*, v. 145, p. 117–152, doi: 10.1016/S0009-2541(97)00159-9.
- Rieck, H.J., Sarna-Wojcicki, A.M., Meyer, C.E., and Adam, D.P., 1992, Magnetostratigraphy and tephrochronology of an upper Pliocene to Holocene record in lake sediments at Tule Lake, northern California: *Geological Society of America Bulletin*, v. 104, p. 409–428, doi: 10.1130/0016-7606(1992)104<0409:MATOAU>2.3.CO;2.
- Rogers, N.W., Thomas, L., Macdonald, R., Hawkesworth, C.J., and Mokadem, F., 2006, ^{238}U - ^{230}Th disequilibrium in recent basalts and dynamic melting beneath the Kenya Rift: *Chemical Geology*, v. 234, p. 148–168, doi: 10.1016/j.chemgeo.2006.05.002.
- Rose, W.I., 1972, Santiaguito volcanic dome, Guatemala: *Geological Society of America Bulletin*, v. 83, p. 1413–1434, doi: 10.1130/0016-7606(1972)83[1413:SVDG]2.0.CO;2.
- Rose, W.I., 1987, Santa María, Guatemala: Bimodal sodarich calc-alkalic stratovolcano: *Journal of Volcanology and Geothermal Research*, v. 33, p. 109–129, doi: 10.1016/0377-0273(87)90056-4.
- Rose, W.I., Grant, N.K., Hahn, G.A., Lange, I.M., Powell, J.L., Easter, J., and Degraff, J.M., 1977, The evolution of Santa María volcano, Guatemala: *The Journal of Geology*, v. 85, p. 63–87.
- Rose, W.I., Hahn, G.A., Drexler, J.W., Malinicono, M.L., Peterson, P.S., and Wunderman, R.L., 1981, Quaternary tephra of northern Central America, *in* Self, S., et al., eds., *Tephra Studies*: Dordrecht, D. Reidel, p. 227–244.
- Sapper, K., 1904, Die vulcanischen Ereignisse in Mittelamerika im Jahre 1902: *Neues Jahrbuch für Mineralogie, Geologie, und Paläontologie*, v. 1, p. 39–90.
- Simkin, T., and Siebert, L., 2000, Earth volcanoes and eruptions: An overview, *in* Sigurdsson, H., et al., eds., *Encyclopedia of volcanoes*: San Diego, Academic Press, p. 249–261.
- Singer, B.S., Thompson, R.A., Dungan, M.A., Feeley, T.C., Nelson, S.T., Picken, J.C., Brown, L.L., Wulff, A.W., Davidson, J.P., and Metzger, J., 1997, Volcanism and erosion during the past 930 ky, at the Tatará-San Pedro complex: Chilean Andes: *Geological Society of America Bulletin*, v. 109, p. 127–142, doi: 10.1130/0016-7606(1997)109<0127:VAEDTP>2.3.CO;2.
- Singer, B.S., Jicha, B.R., Naranjo, J.A., Lara, L.E., Moreno-Roa, H., and Harper, M.A., 2008, Eruptive history, geochronology, and magmatic evolution of the Puyehue-Cordon Caulle volcanic complex, Chile: *Geological Society of America Bulletin*, v. 120, p. 599–618, doi: 10.1130/B26276.1.
- Thouret, J.C., Finizola, A., Fornari, M., Legeley-Padovani, A., Suni, J., and Frechen, M., 2001, Geology of El Misti volcano near the city of Arequipa, Peru: *Geological Society of America Bulletin*, v. 113, p. 1593–1610, doi: 10.1130/0016-7606(2001)113<1593:GOEMVN>2.0.CO;2.
- Vallance, J.W., Schilling, S.P., Matias, O., Rose, W.I., and Howell, M.M., 2001, Volcano hazards at Fuego and Acatenango, Guatemala: U.S. Geological Survey Open-File Report 01-431, 23 p.
- Vogel, T.A., Patino, L.C., Eaton, J.K., Valley, J.W., Rose, W.I., Alvarado, G.E., and Viray, E.L., 2006, Origin of silicic magmas along the Central American volcanic front: Genetic relationship to mafic melts: *Journal of Volcanology and Geothermal Research*, v. 156, p. 217–228, doi: 10.1016/j.jvolgeores.2006.03.002.
- White, S.M., Crisp, J.A., and Spera, F.J., 2006, Long-term volumetric eruption rates and magma budgets: *Geochemistry Geophysics Geosystems*, v. 7, G3, p. Q03010, doi: 10.1029/2005GC001002.
- Williams, S.N., and Self, S., 1983, The October 1902 plinian eruption of Santa María Volcano, Guatemala: *Journal of Volcanology and Geothermal Research*, v. 16, p. 33–56, doi: 10.1016/0377-0273(83)90083-5.
- Woodruff, L.G., Rose, W.I., Jr., and Rigot, W., 1979, Contrasting fractionation patterns for sequential magmas from two calc-alkaline volcanoes in Central America: *Journal of Volcanology and Geothermal Research*, v. 6, p. 217–240, doi: 10.1016/0377-0273(79)90003-9.
- Zimmerman, S.H., Hemming, S.R., Kent, D.V., and Searle, S.Y., 2006, Revised chronology for late Pleistocene Mono Lake sediments based on paleointensity correlation to the global reference curve: *Earth and Planetary Science Letters*, v. 252, p. 94–106, doi: 10.1016/j.epsl.2006.09.030.

MANUSCRIPT RECEIVED 27 OCTOBER 2008
 REVISED MANUSCRIPT RECEIVED 16 APRIL 2009
 MANUSCRIPT ACCEPTED 10 MAY 2009

Printed in the USA